Molecular quantitative trait loci in reproductive tissues impact male fertility in a large mammal

Xena Marie Mapel[1,*], Naveen Kumar Kadri [1,*], Alexander S. Leonard [1], Qiongyu He [1], Audald Lloret-Villas [1], Meenu Bhati [1,$], Maya Hiltpold [1,&], Hubert Pausch [1,#]

[1] Animal Genomics, ETH Zurich, Universitatstrasse 2, 8092 Zurich, Switzerland
[$] current address: Roslin Institute, The University of Edinburgh, Easter Bush Campus, Midlothian EH25 9RG, United Kingdom
[&] current address: GenPhySE, Université de Toulouse, INRAE, ENVT, 31326, Castanet Tolosan, France

[*] equal contribution
[#] Corresponding author

Abstract

Cattle are well suited to investigate inherited variation in male fertility because insemination success is recorded in thousands of artificial insemination bulls. However, functional data from relevant tissues are lacking, which prevents fine-mapping fertility-associated genomic regions to reveal functional links between genotype and phenotype. Here, we profile testis, epididymis, and vas deferens transcriptomes in 118 mature bulls and conduct association tests between 417k molecular phenotypes and 21M genome-wide variants to identify 41k regulatory loci. We show broad consensus in tissue-specific and tissue-enriched gene expression between the three bovine tissues and their human and murine counterparts. Expression- and splicing-mediating variants are more than three times as frequent in testis than epididymis and vas deferens, highlighting the transcriptional complexity of testis. We identify genes (*WDR19*, *SPATA16*, *KCTD19*, *ZDHHC1*) and molecular phenotypes that are associated with male fertility through transcriptome-wide association and colocalization analyses, revealing molecular-genetic underpinnings of quantitative variation in male fertility.

Introduction

Male fertility varies considerably between individuals, but it remains difficult to identify underlying genetic mechanisms (Tüttelmann et al., 2018; Xavier et al., 2021). Exploring the genetic basis of reproductive success requires separating genetic from environmental effects and differentiating between male and female factors that contribute to fertilization; this is only possible when repeated

phenotypic measurements are available for large cohorts. While such cohorts are unavailable for nearly all species, including humans, the beef and dairy industries' reliance on artificial insemination has generated comprehensive catalogs of semen quality and male fertility records for thousands of genotyped artificial insemination bulls (Thibier & Wagner, 2002). Indeed, studies investigating bull fertility have high translational value as they can elucidate evolutionarily conserved functional mechanisms that contribute to undisturbed mammalian fertilization (Lamas-Toranzo et al., 2020; Pausch et al., 2014; Tang et al., 2022), making cattle an unconventional—but ideally suited—species to study the genetic architecture of male reproductive ability.

Bovine male reproductive traits have low-to-moderate heritability, suggesting they are amenable to association testing with dense molecular markers (Butler et al., 2020; Gebreyesus et al., 2021; Nagai et al., 2022; Pausch & Mapel, 2023). Datasets from artificial insemination bulls provide enough statistical power to identify variants that contribute to inherited variation in male fertility through genome-wide association studies (GWAS). Several thousand quantitative trait loci (QTL) for male reproductive traits are listed in the AnimalQTL Database (https://www.animalgenome.org/cgi-bin/QTLdb/index); many of these loci are in non-coding regions of the genome and segregate within populations at relatively high frequencies (Han & Peñagaricano, 2016; Nicolini et al., 2018; Pacheco et al., 2022; Rezende et al., 2018). Though numerous male fertility QTL have been identified in cattle, a lack of functional data has caused the molecular underpinnings for most of these loci to remain elusive (Druet et al., 2009; Hiltpold et al., 2021; Rezende et al., 2018).

Variants that regulate gene expression and splicing influence complex traits and diseases (Garrido-Martín et al., 2021; Y. I. Li et al., 2016; Walker et al., 2019; Yamaguchi et al., 2022). Several Genotype-Tissue Expression (GTEx) projects identified thousands of regulatory molecular quantitative trait loci (molQTL; specifically expression and splicing QTL) throughout mammalian genomes for dozens of tissues (GTEx Consortium, 2020; Liu et al., 2022; The FarmGTEx-PigGTEx Consortium et al., 2022). Integration of molQTL and phenotypic records, or summary statistics from GWAS, through transcriptome-wide association studies (TWAS) can identify regulatory variants that are associated with complex trait variation (Barbeira et al., 2018; Wainberg et al., 2019; Wu et al., 2019). However, since this requires uniform cohorts with detailed trait records and transcriptomics data for functionally relevant tissues, TWAS for male fertility have not been feasible thus far.

69 Here, we establish a large and homogeneous cohort of bulls that contains both DNA sequencing and
70 transcriptome data from testis, epididymis, and vas deferens. We characterize the transcriptomic
71 profile of these three reproductive tissues and identify thousands of loci that influence gene
72 expression and splicing. In doing so, we discover an excess of regulatory small-effect variants in
73 testis that are often tissue specific. Lastly, we conduct transcriptome-wide association studies and
74 colocalization analyses to pinpoint molecular phenotypes that impact bovine male fertility.

75

76 Results

77 We sampled testis, epididymis (caput), and vas deferens tissue from 118 bulls of Braunvieh (BV)
78 ancestry (i.e., Brown Swiss (BS), Original BV (OB), or a cross between one of these and a different
79 breed; Figure 1A;1B;1C; Figure S1). All bulls were considered post-pubertal, although the age at
80 sampling varied from 10 to 37 months. Whole-genome sequencing (WGS) of DNA extracted from
81 testis tissue yielded between 65,207,590 and 461,834,248 cleaned paired-end reads per sample
82 (mean = 208,761,950 ± 63,260,972). The subsequent alignment of these reads against the *Bos taurus*
83 reference genome achieved an average coverage of 12.34 ± 3.71 -fold. Variant calling identified
84 29,660,795 polymorphic sites (single nucleotide polymorphisms (SNPs), insertions and deletions
85 (indels) smaller than 50 bp), of which 21,501,032 met our quality criteria for downstream analyses
86 (Table S1).

87

88 Total RNA from testis, epididymis, and vas deferens tissue was extracted from the same bulls and
89 deeply sequenced with stranded paired-end libraries. We used a splice-aware alignment tool to map
90 an average of 257,050,199, 283,746,666, and 262,089,072 reads per sample for testis, epididymis,
91 and vas deferens, respectively, to the bovine reference genome and the Ensembl gene annotation
92 (Table S2). An additional set of alignments that included WASP filtering (Van De Geijn et al., 2015) to
93 mitigate reference allele bias contained an average of 240,544,139 mapped reads in testis,
94 267,645,035 mapped reads in epididymis, and 251,031,216 mapped reads in vas deferens (Table S2).
95 Our final dataset contained 117, 103, and 84 samples for testis, epididymis, and vas deferens,
96 respectively, 74 of which had data of sufficient quality for all three tissues (Figure 1A; 1B).

97

98 *Gene expression and splicing variation is pervasive in male reproductive tissues*

99 We estimated gene expression in transcripts per million (TPM) and, after filtering, detected 21,844
100 expressed genes (≥ 0.1 TPM and ≥ 6 reads in ≥ 20% of samples) across the three tissues. When
101 considering the three tissues individually, we identified slightly more expressed genes in epididymis

102 (20,376 genes) than in testis and vas deferens (20,222 and 19,051 expressed genes, respectively;
103 Table 1). A majority of expressed genes were found in all three tissues (17,737 genes; Figure 1E) and
104 were protein coding (87.4% – 89.7%; Tables S3). Testis had the most tissue-specific expressed genes
105 (1,106 genes), followed by epididymis (443 genes), and vas deferens (227 genes; Figure 1E).

106

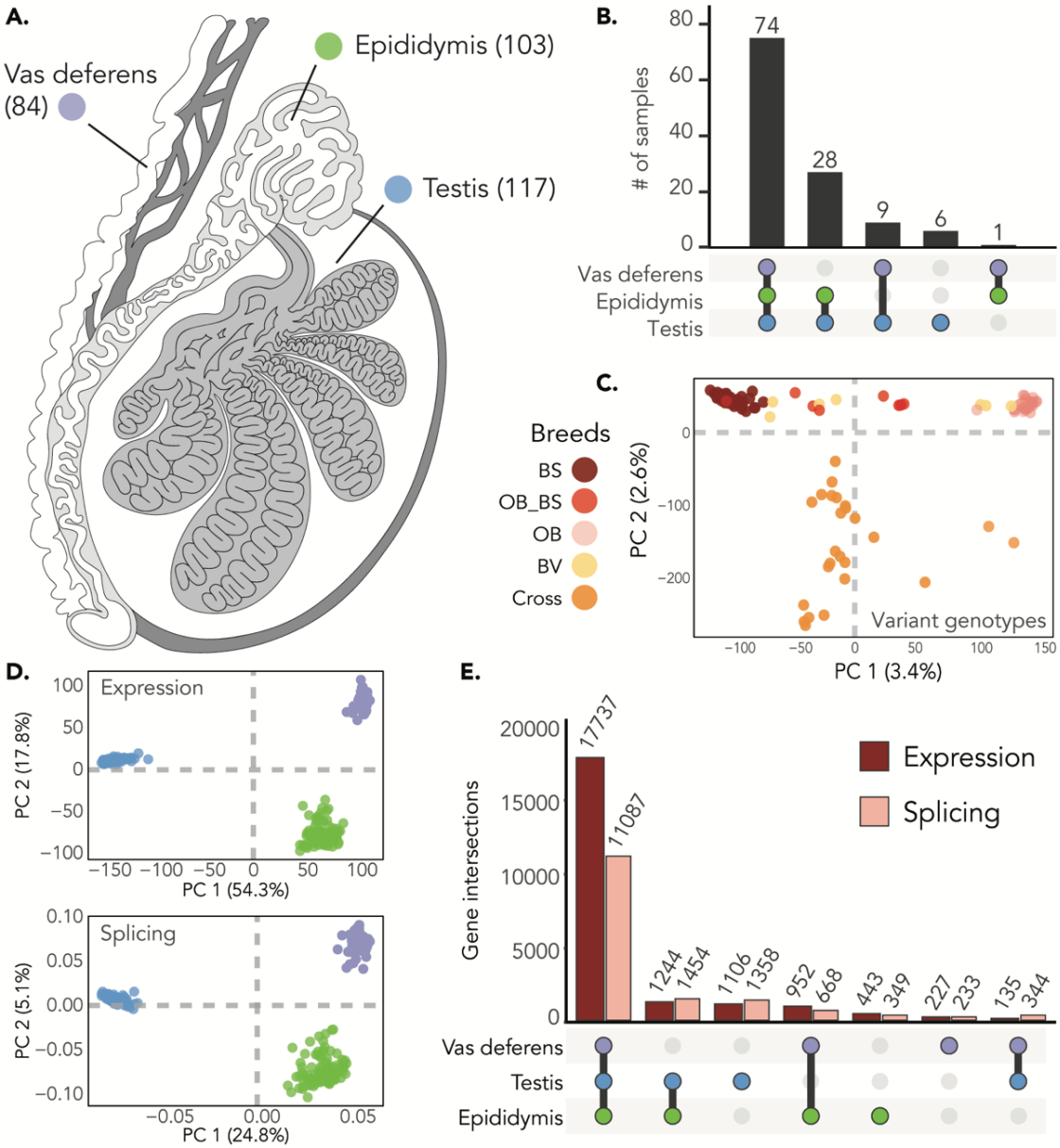

107

108 **Figure 1. Overview of the molQTL cohort for three male reproductive tissues**. A.) The three male
109 reproductive tissues used in our study and the number of samples considered for each tissue. B.) Sample
110 overlap across tissue types. Bar height represents the number of individuals. C.) PCA of LD-pruned sequence
111 variant genotypes (366,090 variants total), with colors corresponding to the breed assigned by the Swiss
112 Braunvieh herd book or "Cross". D.) Scatter plot of the top two principal components of PCAs of normalized
113 expression values (TPM; top panel) and normalized splicing phenotypes (PSI; bottom panel) for all tissues. E).
114 Overlap of expressed and spliced genes across the three tissues (based off the TPM and PSI matrices).

115 **Table 1**. Results for e/sQTL mapping across tissues with a MAF filter of ≥ 1% and FDR of 5%.

	Testis	Epididymis	Vas deferens
Samples	117	103	84
Expressed genes	20,222	20,376	19,063
eQTL	15,642	4,768	4,211
eGenes	11,164	4,347	3,889
eGenes with >1 eQTL	3,647	402	310
eVariants	3,687,265	925,916	673,696
Spliced genes	14,243	13,558	12,332
sQTL	11,450	3,165	1,920
sGenes	7,000	2,662	1,718
sGenes with >1 sQTL	2,849	425	182
sVariants	2,901,402	683,747	313,771

116

117 We examined the tissue specificity of expressed genes following an approach proposed by
118 Djureionovic et al. (2014), which considers genes that are at least 50-fold higher expressed in one
119 tissue compared to other tissues as 'highly tissue-enriched' (Supporting File 1). Genes with critical
120 roles in sperm maturation and the epididymal innate immune response against bacteria (e.g.,
121 *DEFB110*, *DEFB124*, *DEFB121*, *DEFB114*, *WFDC8*, *RNASE10*, *ADAM7*, *ADAM28*, *LCN8*, *LCN10*) were
122 among the 50 most abundant tissue-specific (i.e., not expressed in testis and vas deferens) or highly
123 tissue-enriched transcripts in epididymis. A gene ontology (GO) term enrichment analysis
124 (http://geneontology.org/) revealed that this gene set was 20.57-fold enriched (p = 4.97e-12) for
125 genes related to the GO term "defense response to bacterium". The same gene set enrichment
126 analysis on the 50 most abundant genes that were either specific or enriched in testis (e.g., *INSL3*,
127 *FATE1*, *DEFB123*, *DAZL*, *ARHGAP36*) and vas deferens (e.g., *CD52*, *TNC*, *IGFBP5*, *MMP7*, *HOXD10*,
128 *HOXD11*) did not reveal significant GO terms for either tissue.

129

130 The cattle GTEx consortium analyzed 60 testis transcriptomes (Liu et al., 2022). However, most of
131 them lacked metadata, were collected from pre-pubertal animals, or were from individuals of non-
132 taurine ancestry, precluding an immediate comparison with those from our homogeneous cohort.
133 The abundance of 20,221 testis-expressed genes shared between ten cattle GTEx testis
134 transcriptomes from post-pubertal (1.5 – 9 years) *Bos taurus taurus* bulls and our dataset was highly
135 correlated (Pearson's r = 0.84). The correlation was higher (Pearson's r = 0.90) for 20,002 genes that
136 were expressed with less than 500 TPM in our cohort. The expression of some genes differed
137 between our cohort and the samples included in cattle GTEx (Figure S2), likely due to different RNA
138 sequencing strategies applied to each dataset. The cattle GTEx dataset contained only one vas
139 deferens and two epididymis transcriptomes from adult bulls of taurine ancestry, preventing a
140 meaningful comparison with our data.

141 We compared gene expression in bovine testis, epididymis, and vas deferens with male reproductive
142 tract-specific gene expression in humans and mice (Robertson et al., 2020). Using Ensembl BioMART,
143 we retrieved bovine orthologs for 380 and 329 human and mice reproductive-tract specific genes,
144 respectively, of which the overwhelming majority (92.1% for human; 97.9% for mouse) were also
145 expressed in the three bovine reproductive tissues. A large fraction of the commonly expressed
146 genes was expressed in all three bovine tissues, but testis contributed the most and vas deferens the
147 least number of genes to reproductive tract-specific expression (Figure S3). We observed several
148 differences in gene expression between the species; for instance, *NANOS2,* which is moderately
149 expressed in human testis (13.84 TPM), was barely expressed in bovine reproductive tissue and thus
150 filtered from our dataset. We examined the expression pattern of the bovine orthologs for 220
151 genes that are testis-specific expressed in humans (Djureinovic et al., 2014). The overwhelming
152 majority (218/220) of human testis-specific genes were expressed in bovine reproductive tissue and
153 largely showed testis-biased expression (213/218), although, most were also expressed in bovine
154 epididymis (n=22), vas deferens (n=2), or both other tissues (n=192). We again identified noteworthy
155 differences between the species. Bovine orthologs of two highly expressed testis-specific genes in
156 humans, *DEFB119* encoding defensin beta 119 and *EPPIN* encoding epididymal peptidase inhibitor,
157 were also highly expressed in bovine testis (median TPM *DEFB119* (ENSBTAG00000003364): 64.5;
158 median TPM *EPPIN* (ENSBTAG00000001495): 498.2); however, both genes were three-fold higher
159 expressed in bovine epididymis (median TPM: 217.4 and 1524.3). We detected low and moderate
160 expression of *RNASE11* encoding ribonuclease A family member 11 in epididymis (median TPM:
161 2.18) and vas deferens (median TPM: 19.06) but did not detect any expression in bovine testis tissue
162 despite reports that it is highly tissue-enriched in human testis (Djureinovic et al., 2014).

163

164 We used LeafCutter to detect RNA splicing variation and calculated 'percent spliced-in' (PSI) values
165 for excised-intron clusters. Across the three tissues we observed 15,493 alternatively spliced genes,
166 with 95% of these being protein-coding genes (14,719 genes; Table S3). We detected 11,087 genes
167 that were alternatively spliced in all three tissues. Genes that were alternatively spliced in all three
168 tissues were higher expressed than those for which we did not detect alternative isoforms (Table
169 S4). We identified 139,186 splice junctions and 46,417 intron clusters in testis, 114,343 splice
170 junctions and 44,891 intron clusters in epididymis, and 103,809 splice junctions and 40,480 intron
171 clusters in vas deferens. The total number of genes with alternative splicing events was similar
172 across the three tissues, with 14,243, 13,558, and 12,332 alternatively spliced genes for testis,
173 epididymis, and vas deferens, respectively.

174

175 The similarity of the transcriptional profile of the three male reproductive tissues was assessed
176 through cluster analyses. Principal component analysis (PCA) of normalized expression values (TPM)
177 and splicing phenotypes (PSI) separated samples by tissue type (Figure 1C; 1D), which was further
178 supported by hierarchical clustering (Figure S4). In both expression and splicing PCAs, the first PC
179 separated testis from epididymis and vas deferens, suggesting that the transcriptional profile of
180 testis is distinct from other male reproductive tissues. To further explore the similarity between
181 tissues, we inferred pairwise similarity of gene expression and splice-junction counts with Spearman
182 correlation. For both expression and splicing, vas deferens and epididymis were more similar to each
183 other than to testis (epididymis x vas deferens – expression: $\rho = 0.92$, splicing: $\rho = 0.83$; epididymis x
184 testis – expression: $\rho = 0.82$, splicing: $\rho = 0.67$; vas deferens x testis – expression: $\rho = 0.74$, splicing: ρ
185 $= 0.57$).

186

187 ***Thousands of variants impact gene expression and splicing***

188 To identify loci that influence gene expression (expression QTL, hereafter referred to as eQTL),
189 normalized and standardized TPM values were regressed on variants that had minor allele frequency
190 greater than 1.0% and were within 1 Mb of the annotated transcription start site (TSS). We
191 accounted for covariates such as age, RNA integrity, and hidden confounders that were estimated
192 directly from the data (PEER factors; Figure S5). We identified eQTL in at least one of the three
193 tissues for 12,950 genes (hereafter referred to as eGenes) at a false discovery rate (FDR) of 5%. A
194 majority of eGenes were protein-coding (11,951 eGenes; Table S3). Testis had considerably more
195 eGenes than epididymis and vas deferens (Table 1)—over 55% of genes expressed in testis were also
196 eGenes. Epididymis had 4,347 eGenes (21% of genes expressed in epididymis) and vas deferens had
197 3,889 eGenes (20% of genes expressed in vas deferens). One-third of testis eGenes had more than
198 one independent-acting eQTL (Figure 2A), corresponding to 15,642 eQTL total and 3,687,265 unique
199 significant variants (eVariants). We identified 4,768 independent eQTL (9.2% eGenes having > 1
200 eQTL; Figure 2A) and 925,916 eVariants in epididymis. Vas deferens had the fewest eQTL, with 4,211
201 independent eQTL and 673,696 eVariants. For all tissues, approximately half of all eQTL were within
202 100 kb of the TSS (8,000 testis eQTL; 2,802 epididymis eQTL; 2,423 vas deferens eQTL; Figure S6).

203

204 The effect of each eQTL was quantified as the allelic fold change (slope_aFC) in expression of the
205 associated eGene. The slope_aFC value was highly correlated (Spearman's $\rho \geq 0.84$) with the beta
206 coefficient from the linear model used for eQTL mapping (Figure 2B). Across the three tissues, only
207 2,321 eQTL (9.4%) had large effects (defined as $|\text{slope_aFC} \geq 1|$), with 65% of these loci residing

208 within 100 kb of the eGene's TSS. Notably, testis had the smallest proportion of large effect eQTL
209 (7.58%; 1,186 eQTL; Figure S6). The proportion of large effect eQTL in both epididymis and vas
210 deferens was approximately 12% (599 and 536 eQTL in epididymis and vas deferens, respectively).
211 Large effect eQTL were enriched for low-frequency alleles (Figure S7). We observed that eQTL
212 annotated as non-coding transcript variants had a stronger effect on expression (median slope_aFC
213 = 0.93; Figure 2D).

214

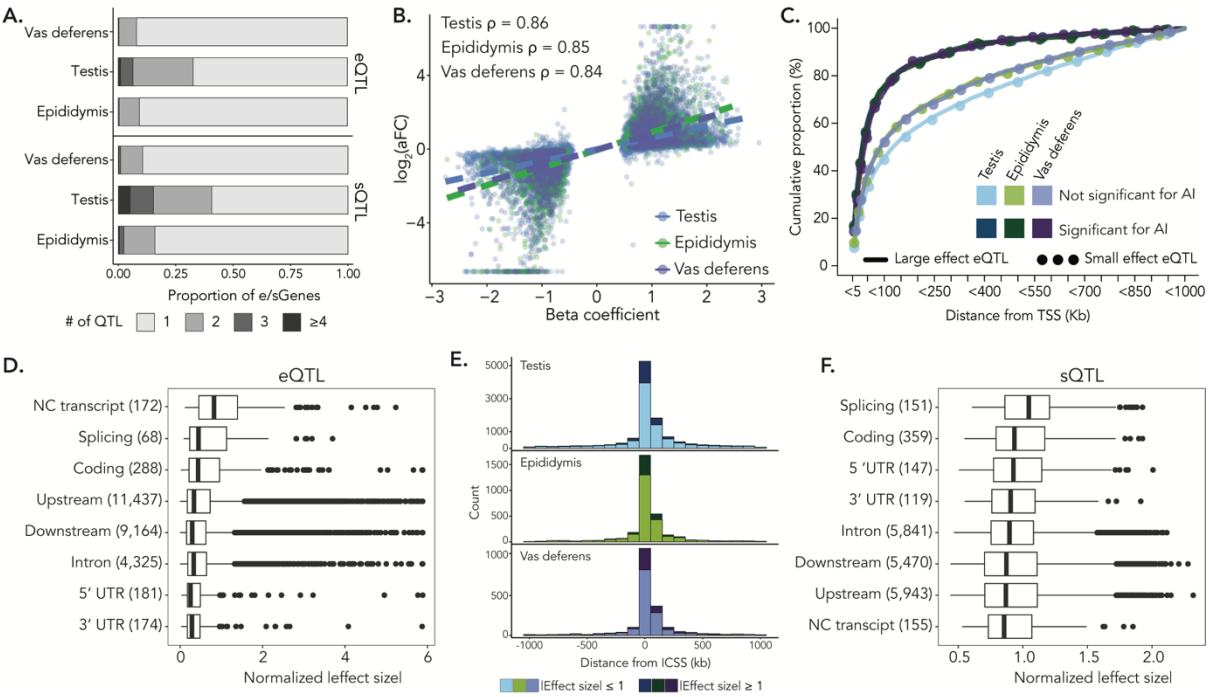

215

216 **Figure 2**. **Properties of eQTL and sQTL in three male reproductive tissues.** A.) Proportion of independent-
217 acting eQTL (top) and sQTL (bottom) across tissues. B.) Correlation (Spearman's ρ) between the β-coefficient of
218 the linear model (used for eQTL identification) and slope_aFC of each eQTL's top eVariant. The linear
219 relationship between the two variables is shown with dotted lines. Colors correspond to the tissue type. C.)
220 Cumulative proportion (%) of eQTL showing significant allelic imbalance in the expression of the associated
221 eGene grouped (in bins of 5 Kb) by their proximity to the transcription start site (TSS). Data for large
222 (|slope_aFC| ≥ 1) and small (|slope_aFC| < 1) effect eQTL are presented separately. Similar data for eQTL not
223 showing significant allelic imbalance are shown for comparison D.) Annotation class of eQTL and rank-
224 normalized absolute effect size for eQTL identified in all three tissues. The number of eQTL within an
225 annotation class is listed in parentheses. E.) Distribution of sQTL (top independent-acting sVariants) from the
226 ICSS for all three tissues. Darker colors represent large effect sQTL (|β-coefficient ≥ 1|). F.) Annotation class of
227 sQTL and rank-normalized absolute effect size for sQTL identified in all three tissues. The number of sQTL
228 within an annotation class is listed in parentheses.

229

230 eQTL are expected to cause an imbalanced expression of the associated gene if they are cis-acting
231 (Aguet et al., 2017; Pirinen et al., 2015). In this scenario, the expression of the associated eGene is
232 influenced only by the linked eQTL allele leading to unbalanced expression of the eGene. Thus, to
233 assess and independently quantify putative cis-regulatory effects of the eQTL, we investigated allelic
234 imbalance in the expression of associated eGenes. In the three tissues between 78 and 80% of the
235 variant-gene pairs were available to this evaluation, of which approximately a quarter (23 – 28%)
236 showed significant evidence of allelic imbalance (FDR < 5%; Wilcoxon rank sum test). The proportion
237 of eGenes that showed allelic imbalance was nearly twice as high (49.8, 46.8, and 47.2% in testis,
238 epididymis, and vas deferens, respectively) for large effect eQTL (|slope_aFC| ≥ 1; n = 1156, 669, 545
239 in testis, epididymis, and vas deferens, respectively (Figure S8B; Figure S8C)). Approximately three
240 quarters (76.53, 76.53, and 74.49% for testis, epididymis, and vas deferens, respectively) of the
241 eGenes with significant allelic imbalance were within 100 kb of the eQTL (Figure 2C). This is between
242 1.26- and 1.44-fold enrichment ($p < 2.16e-16$; Fisher's exact test) compared to random expectation
243 (Figure S8A). The eQTL effect estimated as the magnitude of allelic imbalance (AI_aFC) was strongly
244 correlated with slope_aFC (Spearman's $\rho = 0.69, 0.73, 0.75$ in testis, epididymis, and vas deferens,
245 respectively). The correlation was even stronger (Spearman's $\rho = 0.87, 0.88$ and 0.88 for testis,
246 epididymis and vas deferens, respectively) for a subset of the eQTL where the associated eGenes
247 showed significant allelic imbalance (Figure S8C).

248

249 To identify variants that influence splicing, we conducted sQTL mapping between variants within 1
250 Mb of the intron cluster start site (ICSS) and intron-excision ratios of inferred intron clusters, which
251 were normalized and standardized within and across samples, respectively. We identified 7,777
252 spliced genes across the three tissues with at least one sQTL (sGenes; Table 1) at an FDR of 5%—a
253 majority of which were protein-coding genes (7,471 protein-coding genes; 96% of sGenes). Testis
254 had the most sQTL of the three tissues, further corroborating its transcriptional complexity. We
255 detected 7,000 sGenes in testis, which accounted for nearly half of its alternatively spliced genes. For
256 epididymis and vas deferens, we identified 2,662 and 1,718 sGenes, respectively, corresponding to
257 20% and 14% of their spliced genes. In testis, 40.7% of sGenes had more than one independent-
258 acting sQTL, resulting in 11,450 independent sQTL and 2,901,402 unique significant variants
259 (sVariants; Figure 2A). Fewer sGenes had multiple independent-acting sQTL in epididymis and vas
260 deferens (approximately 16% in epididymis and 11% in vas deferens; Figure 2A); in total, epididymis
261 contained 3,165 sQTL and 683,747 sVariants while vas deferens contained 1,920 sQTL and 313,771
262 sVariants. In all tissues, between 60 and 70% of sQTL were located within 100 kb of the ICSS,

263 corresponding to 6,822, 2,190, and 1,339 sQTL for testis, epididymis, and vas deferens, respectively
264 (Figure 2E).
265
266 sQTL effects were quantified as the regression coefficient from the linear model used for sQTL
267 mapping. There were few large effect sQTL (3,793 sQTL with |β-coefficient| ≥ 1) across the three
268 tissues. Most large effect sQTL were within 100 kb of the ICSS (65%, or 2,476 sQTL across all tissues;
269 Figure 2E). The proportion of large effect sQTL was similar across the three tissues, corresponding to
270 22.7%, 22.5%, and 24.9% of sQTL in testis, epididymis, and vas deferens, respectively (2,603 sQTL in
271 testis, 712 sQTL in epididymis, and 478 sQTL in vas deferens; Figure 2E). We observed that top
272 sVariants within splicing regions—such as splice donor and splice acceptor sites—had the largest
273 effect sizes (median effect size = 1.14; Figure 2F), corroborating that variants overlapping these
274 nucleotides have pronounced impacts on pre-mRNA splicing.
275
276 Identifying distant—or trans—eQTL and sQTL that lie > 5 Mb from a gene's TSS requires larger
277 sample sizes, as they typically have small effects and an increased multiple-testing burden. Thus, we
278 only conducted trans eQTL and sQTL analyses for testis, for which we had the largest number of
279 samples. We observed 76 trans eGenes and 6,038 trans eVariants (FDR 5%) in testis. Most trans
280 eQTL were located on a different chromosome than the target trans eGene (73 trans eGenes and
281 6,024 trans eVariants; Figure S9A). Nearly half (46%; 35 total trans eQTL) of trans eQTL were
282 colocalized (PP4 > 0.8) with at least one cis eQTL, suggesting a complex network of cis mediation. We
283 identified 33 intron clusters with trans sQTL, corresponding to 25 trans sGenes and 1,023 trans
284 sVariants (Figure S9B).
285
286 ***Testis molQTL effects are unique and small, while molQTL effects in other male reproductive***
287 ***tissues are shared***
288 Tissues with similar biological functions often share molQTL (GTEx Consortium, 2020; Liu et al., 2022;
289 Urbut et al., 2019). Thus, we sought to determine if eQTL and sQTL in male reproductive tissues
290 were shared or tissue-specific. We used Mashr to compare molQTL effects for genes that were
291 expressed in all three tissues and considered 11,311 and 5,012 top eVariants and sVariants,
292 respectively. For eQTL, we identified 10,738 variant-gene pairs that were significant in at least one
293 tissue (local false sign rate (LFSR) < 0.05). A large proportion of eQTL were tissue-specific (4,760
294 eQTL; 44% of the eQTL considered), while there was a similar number of eQTL identified in either
295 two or three tissues (two tissues: 2,949 eQTL, 27% of eQTL; three tissues: 3,029 eQTL, 28% of eQTL;

296 Figure 3A). Testis had the most tissue-specific eQTL, followed by vas deferens, and epididymis
297 (Figure 3B). eQTL effects were most similar between vas deferens and epididymis (Spearman's ρ =
298 0.58), and clearly less similar between testis and epididymis (Spearman's ρ = 0.32) and between
299 testis and vas deferens (Spearman's ρ = 0.28). Conversely, most sQTL were ubiquitous—73% of the
300 4,737 variant-gene pairs were significant (LFSR < 0.05) in all tissues (3,451 sQTL; Figure 3A). Only 648
301 sQTL were tissue-specific (14% of sQTL considered; Figure 3A), most of which were in testis (505
302 sQTL; Figure 3B). We observed high pairwise similarity of sQTL effects across the three tissues,
303 particularly between epididymis and vas deferens (testis x epididymis: Spearman's ρ = 0.75; testis x
304 vas deferens: Spearman's ρ = 0.69; epididymis x vas deferens: Spearman's ρ = 0.88).

305

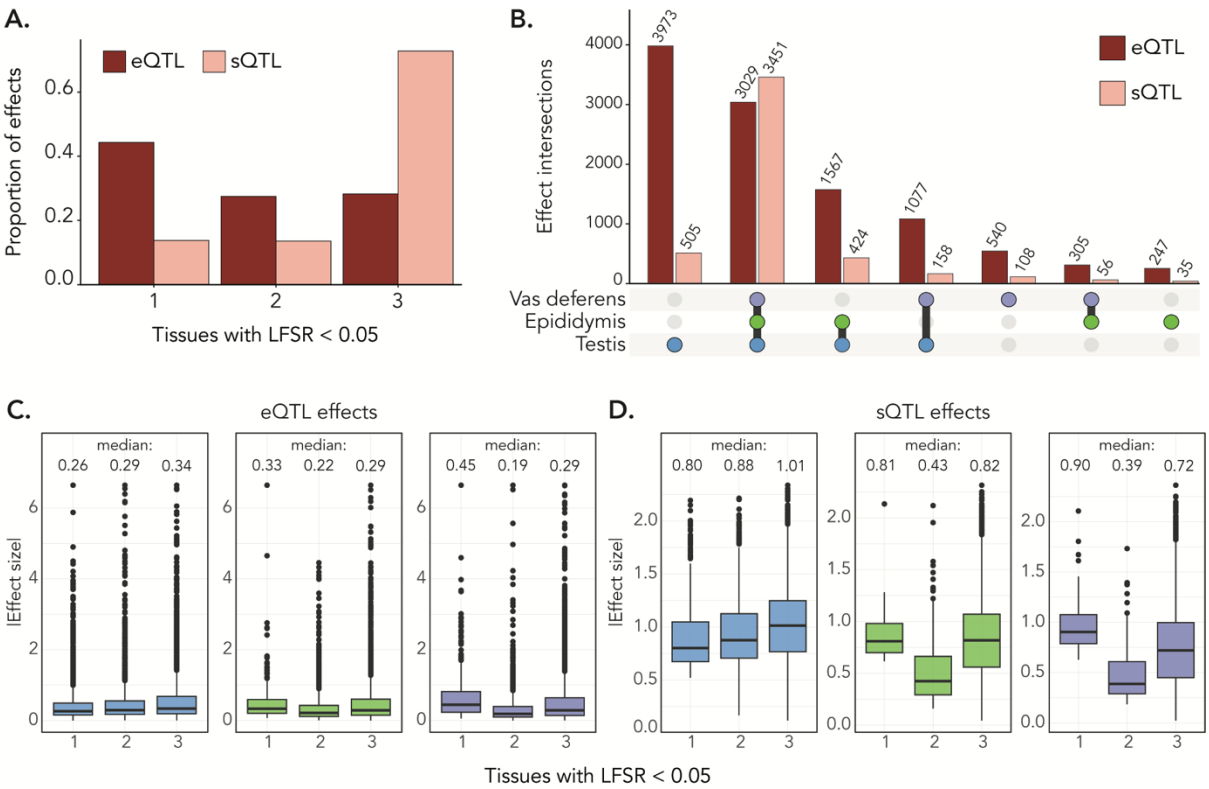

306

307 **Figure 3. Tissue-specific and shared effects of eQTL and sQTL**. A.) Proportion of eQTL and sQTL that are
308 significant (LFSR < 0.05) in one, two, or three tissues. B.) Overlap of significant (LFSR < 0.05) eQTL and sQTL
309 across the three tissues. Bar height represents the number of QTL. C.) Boxplots of the eQTL effect size across
310 tissue specificity classes (significant in one, two, or all three tissues at a threshold of LFSR < 0.05) for testis
311 (blue), epididymis (green), and vas deferens (purple) tissues. Absolute effect size corresponds to |aFC_slope|.
312 Median effect size of each category is included. D.) Boxplots demonstrating the effect size of sQTL across tissue
313 specificity classes for testis, epididymis, and vas deferens tissues. Absolute effect size corresponds to the β-
314 coefficient of the linear model. Median effect size of each category is included.

315

316 Tissue-specific molQTL typically have larger effects than those identified in many, or all, tissues (The
317 FarmGTEx-PigGTEx Consortium et al., 2022; Urbut et al., 2019). We confirmed this phenomenon for
318 epididymis- and vas deferens-specific eQTL, which had larger effects (slope_aFC) than eQTL found in
319 all three tissues (vas deferens: Wilcoxon rank-sum p = 2.48e-16; epididymis: Wilcoxon rank-sum p =
320 0.003; Figure 3C). Vas deferens-specific sQTL also had larger effects than ubiquitous sQTL (Wilcoxon
321 rank-sum p = 7.92e-11), though there was no statistical difference in sQTL effect size across tissue
322 specificity classes for epididymis (Wilcoxon rank-sum p = 0.39). Alternatively, testis specific eQTL and
323 sQTL had smaller effects than those shared across all three tissues (eQTL: Wilcoxon rank-sum p =
324 3.93e-30; sQTL: Wilcoxon rank-sum p = 1.40e-16; Figure 3D), suggesting that testis is composed of
325 many tissue-specific small effect molQTL.
326
327 ***Integration of molecular phenotypes, molQTL, and GWAS summary statistics reveals genes***
328 ***associated with male fertility***
329 We sought to investigate the impact of molQTL on male reproductive ability. First, we conducted
330 GWAS for male fertility with a cohort of 3,736 bulls that had imputed genotypes for 14,587,859
331 SNPs, and separately tested additive and non-additive inheritance. The fertility of the bulls was
332 quantified through the proportion of successful artificial inseminations and accounted for genetic
333 and environmental factors (see Hiltpold et al., 2021). While the GWAS cohort had no overlap with
334 the molQTL cohort, both predominantly consisted of Brown Swiss bulls. Non-additive association
335 testing revealed four male fertility QTL on chromosomes 1, 6, 18, and 26 (significance threshold of
336 5e-08) that contained 4,890 variants (Figure 4A). Additive GWAS did not detect any additional
337 significant associations and failed to identify the QTL on chromosomes 1 and 18. The QTL on
338 chromosomes 6 and 26 were detected by the additive GWAS, but with lower significance (Figure
339 S10).
340
341 We implemented the MetaXcan framework to establish if variation in molecular phenotypes is
342 associated with variation in male fertility. Briefly, S-PrediXcan was used to integrate summary
343 statistics from the non-additive GWAS with expression and splicing phenotypes from the three
344 reproductive tissues. Signals were subsequently filtered based on the colocalization probability
345 between male fertility QTL and molQTL. We identified two and seven unique genes for expression
346 and splicing, respectively, that overlapped three of the male fertility QTL (Figure 4, Table 2). The
347 most striking association was on chromosome 6; *WDR19* encoding WD Repeat Domain 19 was the
348 most significantly associated gene in epididymis and vas deferens (p = 3.17e-43 and 1.04e-48). An
349 intron cluster encompassing a canonical (58373894:58374821) and a cryptic (58373885:58374821)

350 splice junction was the top fertility-associated molecular phenotype in both tissues (Figure S11). A
351 highly significant S-PrediXcan signal (p = 6.10e-38) was also obtained for this *WDR19* intron cluster in
352 testis, however the evidence for colocalization with the GWAS peak was low (PP.H4.abf = 0.39).
353

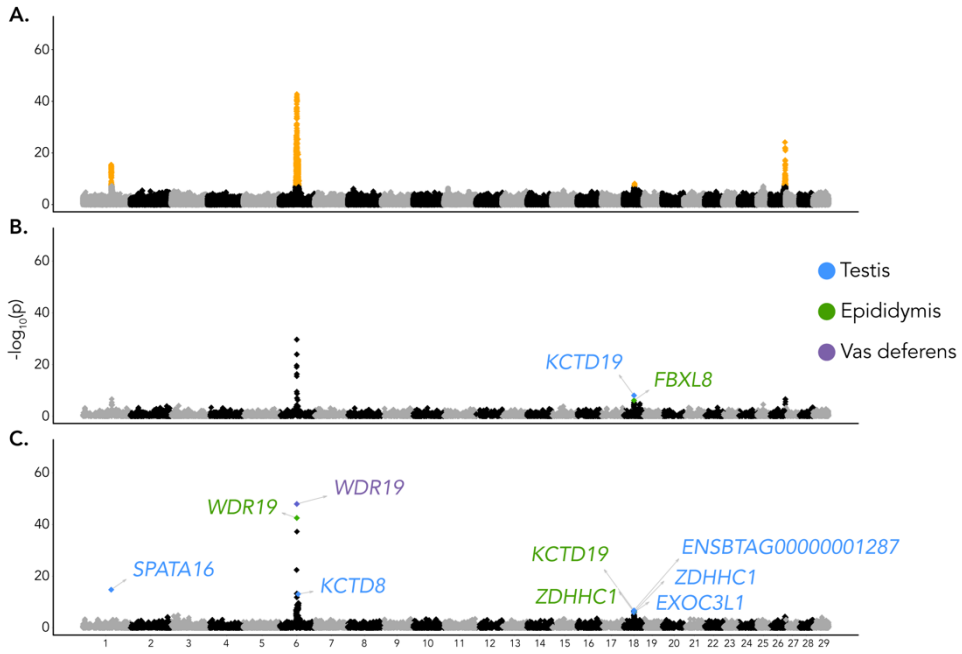

354

355 **Figure 4. Genes associated with male fertility.** Manhattan plots showing genome-wide association between
356 (A) male fertility and imputed sequence variants from non-additive association models. Variants significantly (p
357 < 5e-8) associated with male fertility are highlighted in orange. Transcriptome-wide association with S-
358 PrediXcan between (B) expression values or (C) splicing phenotypes and male fertility. Significantly associated
359 genes after the stringent filtering based on the MetaXcan framework are marked with their names.
360

361 The splicing MetaXcan in testis revealed an association (p = 1.71e-15) between *SPATA16* encoding
362 spermatogenesis associated protein 16 and male fertility (Figure 4C). *SPATA16* mRNA was highly
363 expressed in testis (270.57 ± 32.26 TPM), lowly expressed in epididymis (15.28 ± 9.90 TPM), and
364 barely expressed in vas deferens (1.05 ± 1.18 TPM). Only one *SPATA16* transcript is annotated in
365 Ensembl, but the Refseq annotation suggests three isoforms, of which the canonical isoform
366 (XM_002684936.6) was 12 and 17 times more abundant in testis than two alternative isoforms
367 XM_024995427.1 and XM_005201702.4 (Figure S12A). The fertility-associated *SPATA16* intron
368 cluster comprised four splice junctions that span the first four exons, including a non-coding exon
369 that is only part of the Refseq annotation (Figure 5C; Figure 5D; Figure 5F). The fertility and splicing
370 QTL were colocalized with a probability of 0.86 and a variant (Chr1:93,954,637 bp) 365 kb upstream
371 the annotated *SPATA16* transcription start site was the most probable causal variant (Figure 5A). An

372 association analysis conditional on Chr1:93,954,637 did not identify any additional variants as being
373 associated with male fertility on chromosome 1 (Figure 5B).
374
375 **Table 2**. Male fertility-associated genes prioritized by MetaXcan. P-value is the gene's p-value from S-
376 PrediXcan. PP.H4 is the probability of a shared causal variant for molQTL and QTL from colocalization analysis.
377 Colocalized variant is the most likely colocalized variant from coloc.abf (H4.PP.SNP with largest posterior
378 probability). β–coefficient is the effect estimate of the most likely colocalized variant from the linear model
379 used for molQTL mapping.

Gene	Expression (TPM)			Splice junction and intron cluster	Molecular phenotype	Tissue	P-value	PP.H4	Colocalized variant	β–coefficient
	Testis	Epididymis	Vas deferens							
SPATA16	270.57 ± 32.26	15.28 ± 9.90	1.05 ± 1.18	1:94345963-94396748:clu_3038	Splicing	Testis	1.71E-15	0.86	Chr1: 93,954,637	0.78
WDR19	20.09 ± 2.65	29.46 ± 19.57	36.26 ± 4.82	6:58373894-58374821:clu_63814	Splicing	Epididymis	3.17E-43	0.96	Chr6: 57,900,948	-1.17
				6:58373894-58374821:clu_46646		Vas deferens	1.04E-48	0.99	Chr6: 57,900,948	-1.34
KCTD8	2.71 ± 0.73	0.73 ± 1.00	0.68 ± 0.93	6:62885148-62886027:clu_81370	Splicing	Testis	8.10E-14	0.81	Chr6: 62,206,554	-0.73
KCTD19	238.01 ± 56.20	9.05 ± 6.26	0.58 ± 1.42	--	Expression	Testis	2.27E-07	0.96	Chr18: 34,914,479	1.12
				18:34910787-34910930:clu_25862	Splicing	Epididymis	2.28E-07	0.87	Chr18: 34,914,479	0.67
ZDHHC1	21.96 ± 3.04	24.77 ± 17.29	21.00 ± 3.32	18:35019435-35026730:clu_33937	Splicing	Testis	8.11E-07	0.94	Chr18:34,815,920	-1.12
				18:35019435-35026730:clu_25875		Epididymis	9.44E-07	0.92	Chr18: 34,914,479	-0.81
FBXL8	3.80 ± 1.51	2.05 ± 0.72	1.52 ± 0.46	--	Expression	Epididymis	7.86E-07	0.87	Chr18:35,059,627	0.96
EXOC3L1	13.50 ± 2.15	1.34 ± 0.55	1.73 ± 0.50	18:34825696-34825972:clu_33908	Splicing	Testis	9.91E-07	0.93	Chr18: 34,914,479	0.87
ENSBTAG00000001287	7.17 ± 0.97	3.33 ± 1.00	3.26 ± 0.81	18:34842264-34842709:clu_33910	Splicing	Testis	1.73E-07	0.93	Chr18: 34,815,920	-0.91

380
381
382 The Chr1:93,954,637 T allele compromises male fertility (p = 4.15e-16; Figure 5E) but is associated
383 with increased *SPATA16* mRNA expression (β = 0.71 ± 0.17 TPM_{norm}; p = 6.41e-05)—albeit not at the
384 stringent significance threshold applied to our eQTL analysis (Figure S12B; Figure S12C). Eleven of

385 the twelve *SPATA16* exons were expressed at higher levels in animals carrying the T allele, though
386 this difference was only significant (p = 3.7e-06) for the fourth exon (94,396,748 bp – 94,396,893
387 bp). Interestingly, the second exon (94,323,018 bp – 94,323,140 bp) is the only exon for which
388 abundance is reduced (β = 0.25 ± 0.09 TPM_{norm}; p = 0.0057) by the Chr1:93,954,637 T allele (Figure
389 S12E). This exon is part of SPATA16 isoform XM_024995427.1 but is absent in both the canonical
390 (XM_002684936.6) and another alternative isoform (XM_005201702.4). While the Chr1:93,954,637
391 T allele has no effect on the abundance of the predominant canonical isoform (XM_002684936.6, p =
392 0.15), it increases (β = 3.6 ± 0.68 TPM; p = 6.7e−07) abundance of XM_005201702.4 and reduces
393 abundance of XM_024995427.1 (β = −1.1 ± 0.42 TPM; p = 0.015), suggesting that it promotes
394 differential isoform usage (Figure S12D). This is further supported by an inverse association between
395 inclusion ratios of the second and third exon with the abundance of two alternative SPATA16
396 isoforms (XM_005201702.4 and XM_024995427.1; Figure S13).
397
398 The non-additive GWAS for male fertility revealed a QTL on chromosome 18 (p = 6.41e-09, lead SNP
399 at 36,480,384) that coincides with a previously localized 3 Mb region (between 34 and 37 Mb), for
400 which no compelling candidate causal variants were found (Hiltpold et al., 2021). This 3 Mb window
401 contains 97, 27, and 12 eQTL and sQTL in testis, epididymis and vas deferens, respectively. The
402 MetaXcan and colocalization analyses revealed five significantly associated genes
403 (*ENSBTAG00000001287*, *EXOC3L1*, *FBXL8*, *KCTD19*, *ZDHHC1*) at this QTL, of which *KCTD19* encoding
404 the potassium channel tetramerization domain containing protein 19 shows a highly testis-biased
405 expression (Table 2). Two genes (*KCTD19* and *ZDHHC1* encoding the zinc finger DHHC-type
406 containing protein 1) were each associated with two molecular phenotypes in two tissues. Three
407 variants (Chr18:34,914,479, Chr18:34,815,920, Chr18:35,059,627), which are in moderate LD
408 (between 0.54 and 0.6), are colocalized for the male fertility QTL and seven distinct molecular
409 phenotypes (Table 2). Association analyses conditional on any of these variants did not identify
410 additional variants associated with male fertility on chromosome 18. The Chr18:34,914,479 T allele is
411 associated with higher fertility, an increased KCTD19 mRNA abundance in testis, and the expression
412 of a KCTD19 isoform in the epididymis that has an additional 30 bp coding sequence added to the
413 14th exon which results in a protein that is 10 amino acids longer than that encoded by the canonical
414 form (Figure S14). Alternative *KCTD19* splicing was also highly significant (p = 3.13e–15) in testis, but
415 MetaXcan did not reveal association of this molecular phenotype with male fertility. This variant
416 (Chr18:34,914,479) was also associated with differential *ZDHHC1* splicing in epididymis and
417 differential *EXOC3L1* splicing in testis.
418

419 A QTL (p = 7.59e-23, lead SNP at Chr26:50,145,932) for male fertility was detected on chromosome
420 26. Neither the splicing nor the expression MetaXcan revealed any significant gene-trait associations
421 for this QTL.
422

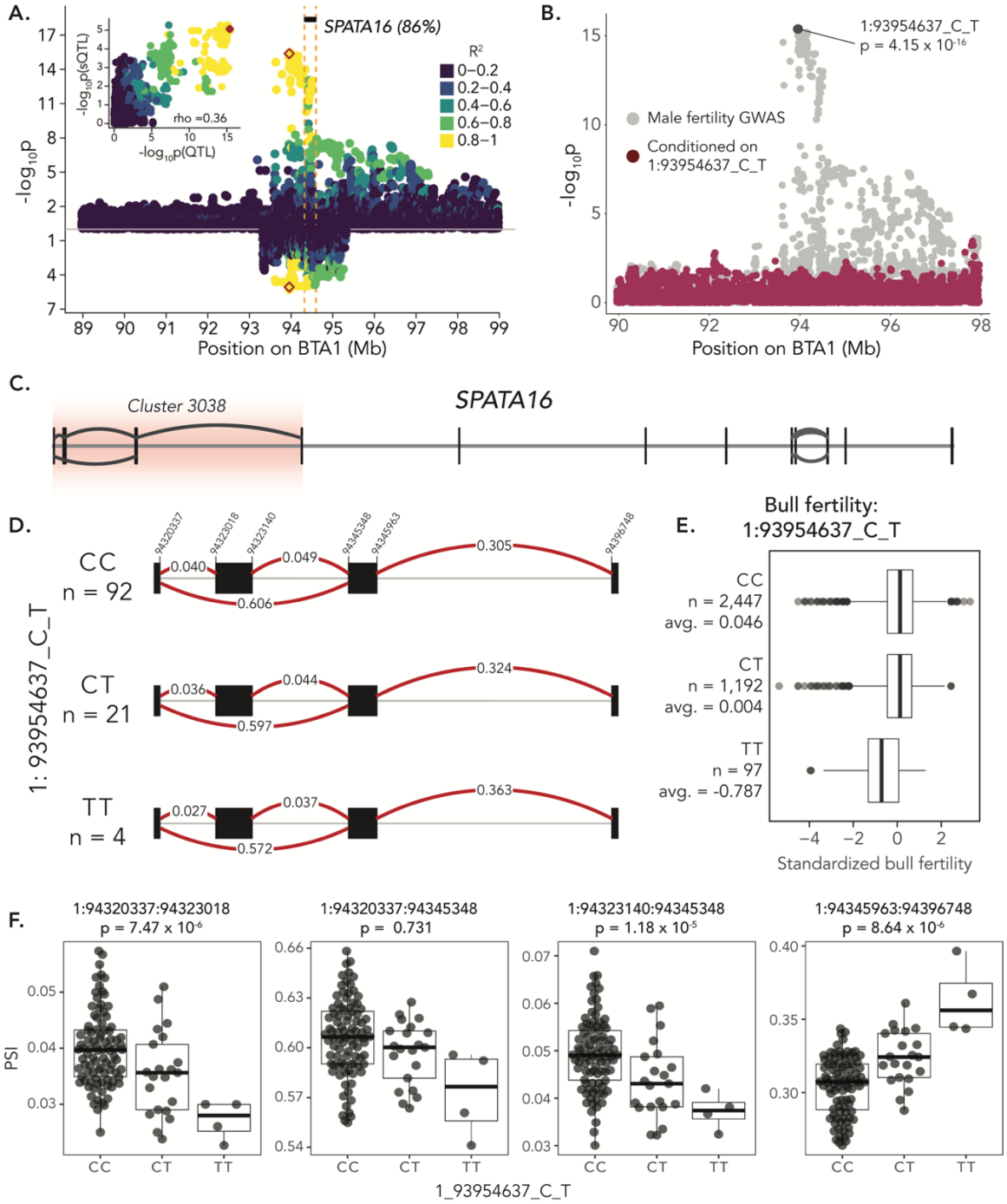

423
424 **Figure 5. A molecular *SPATA16* phenotype overlaps with a male fertility QTL.** A.) Mirrored plots of $-\log_{10}(p)$-
425 values from association testing between imputed sequence variants and bull fertility (top) and splicing
426 phenotypes for intron cluster 3038 of the gene *SPATA16* (bottom). The inset shows the correlation between
427 GWAS and sQTL $-\log_{10}(p)$-values. Color indicates the linkage disequilibrium (R^2) between the most likely
428 colocalized variant (1:93954637_C_T, red colored) and all other variants. B.) Association testing between

429 imputed sequence variants and male fertility before (gray) and after (maroon) conditioning on the genotype of
430 the most likely colocalized variant (1:93954637_C_T). C.) Gene structure of bovine *SPATA16*, showing positions
431 of exons (black lines) and alternative splicing events (arcs). D.) Splicing within *SPATA16* intron cluster 3038 for
432 different genotypes of the top colocalized variant. Red lines show the different splice junctions with the values
433 representing "percent spliced in" estimates within the intron cluster. E.) Standardized bull fertility across the
434 genotypes of the colocalized variant. F.) PSI values for different splicing events within Cluster 3038 across
435 different genotypes of the most likely colocalized variant.
436
437

438 ## Discussion

439 We characterized the transcriptomic profile of testis, epididymis, and vas deferens in a cohort of 118
440 bulls. To the best of our knowledge, a cohort of this size has not been established for male
441 reproductive tissues thus far, though smaller cohorts are available for several species (Djureinovic et
442 al., 2014; Gamble et al., 2020; Zhang et al., 2023). Our molQTL cohort contained bulls within a
443 narrow post-pubertal age range that predominantly belonged to one breed of European taurine
444 cattle. We demonstrated the benefit of establishing such a homogeneous cohort for transcriptome
445 analyses, as we detected 14-times (11,164 vs. 809) more eGenes and 7-times more sGenes (11,450
446 vs. 1,573) in testis than cattle GTEx (Liu et al., 2022) despite our molQTL cohort being only twice as
447 large (117 individuals vs. 60 individuals in cattle GTEx). This suggests that the heterogeneity of cattle
448 GTEx leads to substantial underestimation of the transcriptional complexity of bovine testis and
449 likely other tissues. The number of eGenes and sGenes identified in testis in our study is similar to
450 what was reported in a heterogeneous—but three-times larger—human GTEx cohort (GTEx
451 Consortium, 2020). Comparing our findings with similar-sized cohorts sampled at other
452 developmental stages and the analysis of single-cell transcriptomes will reveal spatiotemporal
453 transcriptomic changes in male reproductive tissue, such as those occurring during testicular
454 development and puberty (Guo et al., 2018, 2020; Liu et al., 2023).
455

456 Our comprehensive set of expressed and spliced genes enabled us to thoroughly characterize and
457 compare the transcriptional complexity of three reproductive tissues in a large mammal, which was
458 so far not possible due to a lack of epididymis and vas deferens data in all existing GTEx cohorts
459 (Robertson et al., 2020). We revealed nearly 20,000 expressed and 14,000 spliced genes within each
460 tissue. Expressed and spliced genes were generally shared across the three reproductive tissues;
461 however, the transcriptional profiles of vas deferens and epididymis were similar, while that of testis
462 was distinct. We found good consensus between pairs of bovine-mouse and bovine-human

463 orthologous genes with male reproductive tract-specific expression, thus demonstrating that our
464 molQTL cohort is a valuable resource for translational research in mammalian male reproductive
465 biology. We observed a similar pattern for eQTL and sQTL—the effects of regulatory variants in vas
466 deferens and epididymis were similar and often shared, whereas testis had a distinct and
467 exceptionally large array of eQTL and sQTL. When compared to the other tissues, we found between
468 3- and 6-times the number of eGenes and sGenes in testis, many of which were regulated by
469 multiple eQTL and sQTL, respectively, which emphasizes its transcriptional complexity that has been
470 reported previously (Ramsköld et al., 2009; Soumillon et al., 2013). Testis contained thousands of
471 tissue-specific, small effect molQTL. An abundance of molQTL in testis was observed in numerous
472 mammalian species (GTEx Consortium, 2020; The FarmGTEx-PigGTEx Consortium et al., 2022),
473 though the reason for this remains unclear. The accumulation of small effect molQTL in testis may be
474 a result of male sexual selection and sperm competition, which is driven by a more permissive
475 transcription (Soumillon et al., 2013), relaxed pleiotropic constraints, and other selective
476 mechanisms (Kaessmann, 2010; Murat et al., 2023). In humans, when compared to other tissues,
477 testis eQTL were more likely to contain signatures of positive selection (Quiver & Lachance, 2022);
478 furthermore, tissue specific eQTL that showed evidence of positive selection had small effect sizes
479 (Quiver & Lachance, 2022). Thus, functional variants in testis may experience unique selection
480 pressures that are essential for male reproduction. Further research is warranted to fully understand
481 the genomic basis of testis's complex functional patterns.
482
483 By leveraging our comprehensive array of molecular phenotypes from reproductive tissues and
484 fertility records from genotyped artificial insemination bulls through gene-based association testing
485 and colocalization analyses, we identified candidate causal regulatory mechanisms underpinning
486 three of the four male fertility QTL. Among them is a previously suspected candidate causal
487 molecular phenotype of *WDR19* (Hiltpold et al., 2020), which adds additional confidence that this
488 approach provides biologically meaningful associations. Our results corroborate that gene splicing
489 and expression variation have substantial effects on complex traits (Xiang et al., 2022) and highlight
490 that regulatory variants need to be considered thoroughly as candidate causal variants. The male
491 fertility QTL were associated with two large effect and one small effect molQTL, thereby
492 demonstrating that molQTL effect size may be a poor predictor of impact on complex trait variation.
493 Spermatogenesis, sperm maturation, and sperm transport are pivotal functions of the three
494 reproductive tissues considered. Gene-based association testing with traits such as sperm
495 morphology or sperm motility may reveal additional gene-trait associations, as they are closer
496 related to the biological function of these tissues than male fertility. However, establishing cohorts

497 with repeated semen quality measurements that are large enough to identify loci that explain only a
498 small proportion of trait variation is challenging in cattle—and almost impossible in most other
499 species.
500
501 We identified an alternative splicing event in testis for *SPATA16* that was significantly associated
502 with male fertility. The colocalized variant fell within an intergenic region between *SPATA16* and
503 *NLGN1*. Previously, a GWAS-only approach prioritized a missense variant of *SPATA16* as a putative
504 causal variant (Hiltpold et al., 2021). However, by combining molecular phenotypes, molQTL
505 analyses, and GWAS—which were appropriately modeled to QTL inheritance—we identified an
506 alternative splicing and regulatory mechanism that is significantly more likely to underpin the QTL.
507 While loss-of-function alleles of *SPATA16* lead to severe sperm defects that prevent fertilization
508 (Dam et al., 2007; Fujihara et al., 2017), our results demonstrate that variants mediating *SPATA16*
509 expression and splicing can contribute to quantitative variation in male fertility as they are less
510 deleterious to protein function. We also identified several gene-trait associations that showed
511 colocalization between molQTL and a non-additive male fertility QTL on chromosome 18. Our
512 inability to resolve this QTL may be due to high linkage disequilibrium or possibly indicates that the
513 causal variant affects multiple genes, as may be the case for large structural variants (Leonard et al.,
514 2023). However, MetaXcan prioritized genes that were previously implicated in male fertility
515 disorders, including *KCTD19* and *ZDHHC1* (Oura et al., 2021; S. Wang et al., 2021; W. Wang et al.,
516 2023). Future fine-mapping efforts that consider additional phenotypic observations and complex
517 genotype variations, such as structural variants called from long read cohorts, will be required to
518 fully describe the molecular underpinnings of this QTL (Leonard et al., 2023).
519
520

521 ## Methods

522 ***Ethics statement***

523 Tissue was sampled at a commercial abattoir. The decision to slaughter the bulls was independent
524 from our study. None of the authors of the present study were involved in the decision to slaughter
525 the bulls. No ethics approval was required for this study.
526

527 ***Tissue sampling and DNA/RNA extraction***

528 Testes from 128 bulls were collected at a commercial abattoir in Zürich, Switzerland after regular
529 slaughter, then transported to a laboratory for preparation. Testis, epididymis (caput), and vas
530 deferens tissue samples were flash-frozen in liquid nitrogen and stored at -80°C until DNA and RNA
531 extraction. The time from slaughter to freezing ranged from 40 minutes to 270 minutes (average:
532 126 minutes ± 47 minutes). Sample collection took place during the fall, winter, and spring of 2019,
533 2020, and 2021. Breed was assigned according to entries from the Swiss Braunvieh herdbook and
534 the animal traffic database.

535

536 We extracted DNA and total RNA from testis tissue with Qiagen AllPrep Mini kits (Qiagen, Hilden,
537 Germany). Frozen testis tissue was homogenized with a MagNA Lyser (Roche, Basel, Switzerland) at
538 6000 rpm for 50 seconds (x2) in RTL Plus Buffer with β-mercaptoethanol. DNA extraction followed
539 standard manufacturer protocols. Concentration was estimated with a Qubit 2.0 fluorometer
540 (Thermo Fisher Scientific) prior to submission for whole genome sequencing (WGS). Extraction of
541 testis total RNA followed manufacturer protocols. Epididymis and vas deferens total RNA was
542 extracted from frozen tissue with Qiagen RNeasy Mini Kits (Qiagen, Hilden, Germany) and included
543 an on-column DNase digestion with Qiagen RNase-Free DNase (Qiagen, Hilden, Germany). Frozen
544 epididymis tissue was homogenized with the same conditions as described for testis tissue. We
545 optimized the homogenization and lysis of vas deferens tissue by adding an additional
546 homogenization period at 6000rpm for 50 seconds and a 60-minute waiting period. We assessed the
547 quality of testis, epididymis, and vas deferens total RNA with an RNA integrity number (RIN) inferred
548 from a Bioanalyzer RNA 600 Nano assay (Agilent Technologies). For subsequent analyses, we only
549 considered samples with RIN > 4.0.

550

551 ***DNA and RNA sequencing***

552 Genomic libraries (paired-end, 150 bp) for WGS were prepared with the Illumina TruSeq DNA PCR-
553 Free protocol and sequenced on two Illumina NovaSeq 6000 S4 flowcells. Paired-end total RNA
554 libraries (150 bp) were prepared with the TruSeq Stranded Total RNA protocol and included rRNA
555 depletion with Ribo-Zero Plus. Libraries were sequenced on four S4 flowcells and one S2 flowcell of
556 the Illumina Novaseq 6000.

557

558 ***DNA alignment and variant calling***

559 We used fastp (v0.19.4; Chen et al., 2018) with default parameters to remove adapter sequences
560 and low-quality bases, and trim poly-G tails from raw DNA sequence data. After quality control, we

561 aligned reads to the ARS-UCD1.2 reference genome (Rosen et al., 2020) with the mem-algorithm
562 from BWA (v0.717; H. Li, 2013) and the -M flag. We sorted the aligned reads by coordinates with
563 Sambamba (v0.6.6; Tarasov et al., 2015), then combined the read-group specific BAM files to create
564 sample-specific sorted BAM files. We marked duplicate reads in the sample specific sorted BAM files
565 with the MarkDuplicates module from Picard tools (https://broadinstitute.github.io/picard/). We
566 used mosdepth (v0.6.6; Pedersen & Quinlan, 2018) to infer the sequencing coverage at a given
567 genomic position, which was then used to estimate the average coverage per sample. Only high-
568 quality reads (mapping quality > 10 or without SAM flag 1796) were considered when calculating the
569 average coverage. We called variants with DeepVariant (v1.3; (Poplin et al., 2018) using the WGS
570 mode. Called samples were merged using GLnexus (v1.4.1; Yun et al., 2020) with the
571 "DeepVariantWGS" configuration. Variants that had a missingness rate greater than 50% and
572 variants for which the genotypes deviated from Hardy-Weinberg proportions (P < 1e-08) were
573 removed. We applied Beagle (v4.1; Browning & Browning, 2016) to impute sporadically missing
574 genotypes and infer haplotypes, then removed sites with model-based imputation accuracy < 0.5. To
575 assess relationships among individuals, we constructed a genomic relationship matrix with 366,090
576 LD-pruned variants (obtained from Plink v1.9 with --indep-pairwise 1000 5 0.2; Chang et al., 2015)
577 that had MAF > 0.5% and performed a PCA with the "pca" function in QTLtools (Delaneau et al.,
578 2017).

579

580 ***RNA alignment***

581 We removed adapter sequences, low-quality bases, poly-A tails, and poly-G tails from the RNA
582 sequence data with fastp. We split cleaned reads into read groups with gdc-fastq-splitter
583 (https://github.com/kmhernan/gdc-fastq-splitter) then aligned them to the cattle reference genome
584 (ARS-UCD1.2) and the Ensembl gene annotation (release 104) with STAR (version 2.7.9a; Dobin et al.,
585 2013). To account for allelic mapping bias in the sQTL and allele specific expression (ASE) analyses,
586 we produced additional alignments with the flag --waspOutputMode and heterozygous SNPs. We
587 performed coordinate sorting and added read groups with Picard
588 (https://broadinstitute.github.io/picard/). We merged each sample's BAM files with Sambamba
589 (v0.6.6; Tarasov et al., 2015) and marked duplicate reads with the MarkDuplicates module from
590 Picard (https://broadinstitute.github.io/picard/). Statistics on the alignment quality were inferred
591 with the flagstat function from Sambamba for each sample.

592

593 ***Expression and splicing quantification***

594 We quantified gene-level expression with the "quan" function in QTLtools. We produced gene-level
595 TPM values with high quality reads that passed all alignment quality filters and only included reads
596 that were uniquely mapped and properly paired. Gene-level read counts were inferred with
597 featureCounts (Liao et al., 2014). We filtered expression values for each tissue to include genes with
598 expression ≥ 0.1 TPM and ≥ 6 reads in ≥ 20% of samples. The filtered expressed genes were inverse
599 normal transformed and quantile normalized for subsequent analyses (Robinson & Oshlack, 2010).
600 To observe clustering within and across tissue types, we used the filtered, normalized TPM values to
601 perform a PCA and hierarchical clustering with the dendextend (v1.16.0) package in R.

602

603 To infer splicing events, we quantified intron-excision values for identified intron clusters. We
604 extracted exon-exon junctions from reads that passed WASP filtering with Regtools (Cotto et al.,
605 2023) and considered a minimum anchor length of 8 bp, minimum intron size of 50 bp, and
606 maximum intron size of 500,000 bp. Intron clustering, calculation of intron excision ratios, filtering,
607 and preparation for sQTL mapping was performed with Leafcutter (Y. I. Li et al., 2018) and executed
608 with the cluster_prepare_fastqtl.py wrapper provided by the human GTEx consortium
609 (https://github.com/broadinstitute/gtex-pipeline/tree/master/qtl/leafcutter). We assigned clusters
610 to annotated genes with an altered map_clusters_to_genes.R script that accounted for strandedness
611 and gene coordinates from a collapsed gene annotation for cattle (Ensembl release 104; generated
612 with scripts from https://github.com/broadinstitute/gtex-pipeline/tree/master/gene_model). We
613 limited our dataset to high-quality introns by imposing stringent filters that removed introns without
614 read counts in > 50% of samples, introns with low variability across samples, and introns with fewer
615 than max (10, 0.1*n*) unique values (where *n* is sample size). To normalize the filtered counts and
616 produce files for sQTL mapping, we used the prepare_phenotype_table.py script from Leafcutter.
617 We performed hierarchical clustering and conducted a PCA on the resulting normalized intron
618 excision phenotypes and hierarchical clustering with the dendextend package in R.

619

620 ***eQTL mapping, allelic imbalance, and sQTL mapping***

621 eQTL mapping was performed for all three tissues with QTLtools. To account for population
622 structure and other covariates that influence gene expression, normalized expression phenotypes
623 were corrected with the first three genotype PCs, ten PEER (Stegle et al., 2012) factors (estimated
624 for each tissue of interest; Figure S5), the age of the individual, and RIN value of the sample. We
625 considered sequence variants with MAF > 1% and included variants 1 Mb up- and downstream of the
626 transcription start site (TSS). To account for multiple testing, we used the "permute" function in

627 QTLtools to conduct 1000 permutations and produce beta corrected p-values. We used the adjusted
628 p-values and the qtltools_runFDR_cis.R script to apply a false discovery rate (FDR) threshold of 5%
629 and identify expressed genes with at least one significant eQTL. To identify all significant variant-
630 gene pairs, we followed the procedure detailed in Delaneau et al., (2017). Specifically, each gene's
631 beta p-values and most-likely beta parameters were used with the FDR level to feed the beta
632 quantile function. This generated nominal p-value thresholds for each expressed gene, and all
633 variants below this threshold were deemed significant. To identify genes with multiple independent
634 acting eQTL, we implemented the conditional analysis from QTLtools. Briefly, this process uses the
635 aforementioned nominal p-value thresholds to identify all significant eVariants, then implements
636 forward and backward stepwise linear regression to identify independent acting eQTL. The
637 significant eVariants are then assigned to the independent signals.

638

639 To estimate the effect size of significant eQTL, we computed the log allelic fold change (slope_aFC;
640 Mohammadi et al., 2017) with aFC.py (https://github.com/secastel/aFC) for the top variant of each
641 independent eQTL. We used gene counts from featureCounts, which were normalized with DESeq2
642 (Love et al., 2014) and log transformed. We compared the normalized eQTL effect sizes to the
643 annotation category of the top variant (obtained with the Variant Effect Predictor (VEP) from
644 Ensembl; McLaren et al., 2016 et al., 2016) to investigate functional consequences.

645

646 We studied allelic imbalance using RNA sequencing reads filtered with WASP (Van De Geijn et al.,
647 2015) to mitigate reference allele bias. Whole genome DNA sequence data phased with beagle 5.4
648 (Browning et al., 2021) were complemented with the "read backed phasing" of the RNA seq data
649 using phASER (Castel et al., 2016) with the flag --baseq 10. Sequencing reads overlapping
650 heterozygous sites within protein coding genes (Ensembl version 104) were used to produce gene
651 level haplotypic expression counts using phASER_gene_AE.py with the –min_haplo_maf 0.005 flag. A
652 median number of 3,834, 3,345, and 1,353 RNA sequencing reads per gene, and 6,352,369,
653 8,453,661 and 6,739,602 reads per sample covering the heterozygous sites of the protein coding
654 genes were available in testis, epididymis, and vas deferens, respectively. Haplotype expression
655 counts across all samples were compiled using phaser_expr_matrix.py to validate cis-regulatory
656 effects of eQTL identified in the three tissues and to independently estimate their effects. eGenes
657 harboring heterozygous sites covered with at least 8 sequencing reads and top eVariants with at
658 least 10 homozygous and 10 heterozygous individuals were considered for this assessment, resulting
659 in a subset of 12,261, 3,832, and 2,871 variant-gene pairs in testis, epididymis, and vas deferens,
660 respectively. Gene level haplotypes were then phased with their associated top eVariant using

661 phaser_cis_var.py. Individual level magnitude of allelic imbalance was estimated as log allelic fold
662 change (AI_aFC) using phaser_cis_var.py. The AI_aFC is the ratio of gene haplotype counts linked to
663 alternative allele to the gene haplotype counts linked to the reference allele of the top eVariant on
664 log2 scale. The median of AI_aFC in individuals heterozygous for the top eVariant is presented as an
665 independent estimate of the cis regulatory effect of that eQTL. Comparison of AI_aFCs in individuals
666 heterozygous for the top eVariant allelic imbalance expected) and homozygous for the top eVariant
667 (allelic imbalance not expected) was used to test the significance of allelic imbalance using a
668 Wilcoxon ranksum test implemented in phaser_cis_var.py.
669
670 sQTL mapping was performed with QTLtools and generally followed the approach used for eQTL
671 discovery. However, we used the "grp-best" option to adjust the permutation scheme to correct for
672 multiple splice junctions and intron clusters within a gene. Mapping was conducted with variants 1
673 Mb up and downstream of the TSS and we included three genotype PCs, age, RIN, and ten PEER
674 factors as covariates. We conducted the QTLtools conditional analysis to identify all significant
675 variants (sVariants) and independent acting sQTL. We considered the β–coefficient from the
676 QTLtools linear model for the top sVariant as the sQTL effect size. Normalized sQTL effect sizes were
677 compared across VEP functional annotation categories using the previously described variant
678 annotation classes.
679
680 Trans eQTL and sQTL were only mapped for testis. We considered 5,685,508 variants that had MAF >
681 5%, were outside of repetitive regions (identified by RepeatMasker (v4.1.4);
682 http://www.repeatmasker.org), had imputation accuracy of 1.0, and had mappability > 1. Variant
683 mappability was determined with GenMap (v1.3.0; Pockrandt et al., 2020) using kmers with lengths
684 of 36 for UTRs and 75 for exons (based on the ARS-UCD1.2 reference) and allowed for two
685 mismatches. We mapped trans QTL for protein coding genes that had a mappability > 0.80 (18,876
686 genes). Gene mappability was estimated with crossmap (https://github.com/battle-lab/crossmap;
687 Saha & Battle, 2019). Phenotypes (either TPM values or PSI values) were corrected for the same
688 covariates used in the cis analysis and rank normal transformed. We used the "trans" function from
689 QTLtools to identify QTL > 5Mb from a gene's TSS and performed 100 permutations, which were
690 then ranked and used to estimate FDR. We considered a trans eVariant or sVariant significant if it
691 had an FDR < 0.05. We removed trans QTL that were cross-mapped (https://github.com/battle-
692 lab/crossmap; Saha & Battle, 2019). Due to excessive linkage observed in cattle, we removed trans
693 QTL with variants that had LD > 0.01 with eQTL or sQTL for those eGenes or sGenes, respectively.
694

695 ***Shared eQTL and sQTL***

696 We identified shared and tissue specific QTL with Mashr (v0.2.69; Urbut et al., 2019). We included
697 top eVariants and sVariants from genes that were expressed in all three tissues. To prevent the
698 double-counting of molQTL that are in linkage disequilibrium and impact the same gene or intron
699 cluster, we selected a single top molQTL that had the largest effect across tissues (as described in
700 Urbut et al., 2019). This resulted in 11,311 eVariants and 5,012 sVariants. We considered a subset of
701 200,000 randomly selected variants and invoked a threshold of LFSR < 0.05 to establish if an effect
702 was significant in a tissue. For significant effects, we assessed pairwise tissue similarity with
703 Spearman's correlation. We compared the magnitude of molQTL effect sizes across specificity
704 classes (tissue specific, in two tissues, or in all tissues) for each tissue with a Wilcoxon signed rank
705 test.

706

707 ***GWAS of male fertility***

708 Genome-wide association tests assuming additive and non-additive modes of inheritance were
709 carried out between imputed genotypes and estimates of sire insemination success (which we used
710 as a proxy for "male fertility"; Hiltpold et al., 2021) in 3,736 bulls using GCTA (Yang et al., 2011). The
711 additive association testing was carried out using additively coded SNP genotypes. For the non-
712 additive association testing, SNP genotypes were coded assuming recessive inheritance to the
713 reference (R) allele and alternate (A) allele. Genotypes were coded as RR = 1, RA = 0, AA = 0 (M1) in
714 the former case and as AA = 1, RA = 0, RR = 0 (M2) in the latter case. Only SNPs with MAF > 0.5% and
715 where the frequency of 1's was between 0.5% and 0.95% (N = 14,587,856) were retained for
716 association testing. The smallest P value from M1 and M2 was considered as the strength of non-
717 additive association between genotypes and phenotypes for each of the tested variant, and variants
718 with P < 5e-08 were considered significant. A genomic relationship matrix constructed from
719 18,187,234 autosomal SNPs with MAF > 0.005 was included in the association model to control for
720 relatedness among samples.

721

722 ***Integrating QTL and molQTL in MetaXcan framework***

723 We used S-PrediXcan (Barbeira et al., 2018) to test for an association between molecular
724 phenotypes (expression and splicing phenotypes) and male fertility. The summary statistic-based
725 approach was applied to include results from non-additive association testing. Briefly, we trained
726 elastic-net based prediction models for expression values (TPM) and splicing phenotypes (PSI),
727 respectively, for all genes and intronic clusters separately in testis, epididymis, and vas deferens.

728 SNPs located within 1 Mb of the TSS of the genes were considered for training with the script
729 gtex_tiss_chrom_training.R. In total, 18,053,560 sequence variants (MAF > 1%) called in the molQTL
730 cohort were available for training the prediction models. Covariates used in the eQTL and sQTL scans
731 were included in training of respective prediction models to account for confounding factors. High-
732 performance prediction models (zscore_pval < 0.05 and rho_avg > 0.1) were available to predict
733 expression levels of 15,810 genes and to predict splicing phenotypes for 46,426 intron clusters
734 across three tissues (77, 80, and 58% of eGenes and for 92, 94, and 80% of intron clusters in testis,
735 epididymis, and vas deferens respectively). Using weights for each SNPs in these high-performance
736 prediction models, we then carried out gene level and cluster level association test for expression
737 and splicing phenotype respectively using the script SPrediXcan.py. Following the recommendations
738 in Barbeira et al., (2018), Bonferroni-corrected P values of 3.16e-06 (0.05/15,810) and 1.08e-06
739 (0.05/46,426), respectively considering the number of genes and intron clusters tested for
740 expression and splicing phenotypes, were set as a significant threshold. Further, a filter was applied
741 on the prediction performance of the model with the threshold set at 0.05/number of significant
742 results after the previous filtering.

743 Next, to avoid capturing LD-contaminated associations, as recommended in the MetaXcan
744 framework (Barbeira et al., 2018), we carried out Bayes Factor colocalization analyses with the R
745 package coloc (Giambartolomei et al., 2014). For every significant GWAS signal (p < 5e-08), we
746 searched for evidence of its colocalization with molQTL using the “coloc.abf” function. The search
747 space was limited to 5 Mb up- and downstream of the significant GWAS peaks. Colocalizations with
748 PP.H4.abf (probability of a shared causal variant) > 0.8 and PP.H3.abf (probability of different causal
749 variants) < 0.5 were retained and used to filter TWAS results.

750

751 ***Characterization of a SPATA16 sQTL***

752 The Ensembl annotation of *SPATA16* contains only one transcript, whereas the Refseq annotation
753 suggests three isoforms (XM_002684936.6, XM_024995427.1, XM_005201702.4) that differ in both
754 the number of coding and the number of non-coding exons. The abundance of the three isoforms
755 was quantified with kallisto (Bray et al., 2016). Testis RNA sequencing data was processed and
756 aligned to the cattle reference genome (ARS-UCD1.2) and the Refseq gene annotation (version 106)
757 with STAR (see above). Exon-specific SPATA16 expression was quantified with QTLtools "quan" on
758 the STAR-aligned bam files (see above). Association tests between exon expression and
759 Chr1:93,954,637 were conducted with a linear model in R that considered three PCs, age, and RIN as
760 covariates. Bonferroni correction was applied to determine a significance threshold with 0.05/n,
761 where n is the number of exons tested.

762 ## Data availability

763 DNA and RNA sequencing data of 118 bulls are available in the ENA database at the study accessions
764 PRJEB28191 and PRJEB46995. Gene expression and splicing matrices, a VCF file of genome-wide
765 genotypes used for e/sQTL mapping, a cross-table to link genotype and transcriptome data, as well
766 as summary statistics used for transcriptome-wide association testing have been archived at zenodo
767 (https://doi.org/10.5281/zenodo.8093287).
768

769 ## Author contributions

770 XMM sampled tissue and established the molQTL cohort, aligned RNA sequencing data, quantified
771 gene expression and splicing variation, developed workflows and applied them to map e/sQTL,
772 contributed to the TWAS, interpreted results, and drafted the manuscript; NKK imputed sequence
773 variant genotypes, established workflows for GWAS, conducted ASE analyses and TWAS, contributed
774 to eQTL analysis, interpreted results, and contributed to the writing of the manuscript; NKK and
775 XMM performed colocalization analyses; MH coordinated the sampling of tissue with the abattoir
776 staff, sampled tissue, and prepared phenotype data; ALV contributed to short read alignment; ASL
777 performed variant discovery and genotyping, and contributed to e/sQTL mapping; QH contributed to
778 GWAS; MB performed the WASP alignment of the RNA-seq data and contributed to discussions
779 about the molQTL mapping workflows; HP conceptualized the study, contributed to the molQTL fine-
780 mapping, interpreted results, and contributed to the writing of the manuscript; all authors read and
781 approved the final version of the manuscript.
782

783 ## Acknowledgements

784 We appreciate support from the abattoir veterinarians and staff as well as Till Graf, Patrick Fitzi, and
785 Remo Hengartner for assistance with tissue sampling. We thank Dr. Fritz-Schmitz Hsu and Dr. Ulrich
786 Witschi (Swissgenetics) for providing phenotype data. We thank Braunvieh Schweiz for providing
787 genotype data of Swiss BSW bulls. We acknowledge the Arbeitsgemeinschaft Deutsches Braunvieh,
788 Braunvieh Austria, Tierzuchtforschung Grub, the Chair of Animal Breeding of TU München, the
789 Institute of Animal Breeding from Bayerische Landesanstalt für Landwirtschaft and ZuchtData EDV
790 Dienstleistungen GmbH for providing genotype and phenotype data of Austrian and German BSW
791 bulls. We thank the Functional Genomics Center Zurich (Dr. Catharine Aquino) for generating DNA
792 and RNA sequencing data. We thank Dr. Jeremie Vandenplas (Wageningen University & Research,
793 Wageningen, the Netherlands) for providing a modified version of the GCTA tool that allows
794 considering allele dosage data.
795

Funding

This study was supported by grants from the Swiss National Science Foundation, an ETH Research Grant, Swissgenetics, and the European Union's Horizon 2020 research and innovation programme under Grant Agreement No. 815668 (BovReg). The funding bodies were neither involved in the design of the study and collection, analysis, and interpretation of data nor in writing the manuscript.

References

Aguet, F., Brown, A. A., Castel, S. E., Davis, J. R., He, Y., Jo, B., Mohammadi, P., Park, Y. S., Parsana, P., Segrè, A. V., Strober, B. J., Zappala, Z., Cummings, B. B., Gelfand, E. T., Hadley, K., Huang, K. H., Lek, M., Li, X., Nedzel, J. L., … Zhu, J. (2017). Genetic effects on gene expression across human tissues. *Nature*, *550*(7675), 204–213. https://doi.org/10.1038/nature24277

Barbeira, A. N., Dickinson, S. P., Bonazzola, R., Zheng, J., Wheeler, H. E., Torres, J. M., Torstenson, E. S., Shah, K. P., Garcia, T., Edwards, T. L., Stahl, E. A., Huckins, L. M., Aguet, F., Ardlie, K. G., Cummings, B. B., Gelfand, E. T., Getz, G., Hadley, K., Handsaker, R. E., … Im, H. K. (2018). Exploring the phenotypic consequences of tissue specific gene expression variation inferred from GWAS summary statistics. *Nature Communications*, *9*(1), 1–20. https://doi.org/10.1038/s41467-018-03621-1

Bray, N. L., Pimentel, H., Melsted, P., & Pachter, L. (2016). Near-optimal probabilistic RNA-seq quantification. *Nature Biotechnology*, *34*(5), 525–527. https://doi.org/10.1038/nbt.3519

Browning, B. L., Tian, X., Zhou, Y., & Browning, S. R. (2021). Fast two-stage phasing of large-scale sequence data. *American Journal of Human Genetics*, *108*(10), 1880–1890. https://doi.org/10.1016/j.ajhg.2021.08.005

Butler, M. L., Bormann, J. M., Weaber, R. L., Grieger, D. M., & Rolf, M. M. (2020). Selection for bull fertility: A review. *Translational Animal Science*, *4*(1), 423–441. https://doi.org/10.1093/TAS/TXZ174

Castel, S. E., Mohammadi, P., Chung, W. K., Shen, Y., & Lappalainen, T. (2016). Rare variant phasing and haplotypic expression from RNA sequencing with phASER. *Nature Communications*, *7*. https://doi.org/10.1038/ncomms12817

Chang, C. C., Chow, C. C., Tellier, L. C. A. M., Vattikuti, S., Purcell, S. M., & Lee, J. J. (2015). Second-generation PLINK: Rising to the challenge of larger and richer datasets. *GigaScience*, *4*(1). https://doi.org/10.1186/s13742-015-0047-8

Chen, S., Zhou, Y., Chen, Y., & Gu, J. (2018). Fastp: An ultra-fast all-in-one FASTQ preprocessor. *Bioinformatics*, *34*(17), i884–i890. https://doi.org/10.1093/bioinformatics/bty560

830 Cotto, K. C., Feng, Y.-Y., Ramu, A., Richters, M., Freshour, S. L., Skidmore, Z. L., Xia, H., McMichael, J.
831 F., Kunisaki, J., Campbell, K. M., Chen, T. H.-P., Rozycki, E. B., Adkins, D., Devarakonda, S.,
832 Sankararaman, S., Lin, Y., Chapman, W. C., Maher, C. A., Arora, V., … Griffith, M. (2023).
833 Integrated analysis of genomic and transcriptomic data for the discovery of splice-associated
834 variants in cancer. *Nature Communications*, *14*(1), 1589. https://doi.org/10.1038/s41467-023-
835 37266-6
836 Dam, A. H. D. M., Koscinski, I., Kremer, J. A. M., Moutou, C., Jaeger, A. S., Oudakker, A. R., Tournaye,
837 H., Charlet, N., Lagier-Tourenne, C., Van Bokhoven, H., & Viville, S. (2007). Homozygous
838 mutation in SPATA16 is associated with male infertility in human globozoospermia. *American*
839 *Journal of Human Genetics*, *81*(4), 813–820. https://doi.org/10.1086/521314
840 Delaneau, O., Ongen, H., Brown, A. A., Fort, A., Panousis, N. I., & Dermitzakis, E. T. (2017). A
841 complete tool set for molecular QTL discovery and analysis. *Nature Communications*, *8*.
842 https://doi.org/10.1038/ncomms15452
843 Djureinovic, D., Fagerberg, L., Hallström, B., Danielsson, A., Lindskog, C., Uhlén, M., & Pontén, F.
844 (2014). The human testis-specific proteome defined by transcriptomics and antibody-based
845 profiling. *Molecular Human Reproduction*, *20*(6), 476–488.
846 https://doi.org/10.1093/molehr/gau018
847 Dobin, A., Davis, C. A., Schlesinger, F., Drenkow, J., Zaleski, C., Jha, S., Batut, P., Chaisson, M., &
848 Gingeras, T. R. (2013). STAR: Ultrafast universal RNA-seq aligner. *Bioinformatics*, *29*(1), 15–21.
849 https://doi.org/10.1093/bioinformatics/bts635
850 Druet, T., Fritz, S., Sellem, E., Basso, B., Gérard, O., Salas-Cortes, L., Humblot, P., Druart, X., & Eggen,
851 A. (2009). Estimation of genetic parameters and genome scan for 15 semen characteristics
852 traits of Holstein bulls. *Journal of Animal Breeding and Genetics*, *126*(4), 269–277.
853 https://doi.org/10.1111/j.1439-0388.2008.00788.x
854 Fujihara, Y., Oji, A., Larasati, T., Kojima-Kita, K., & Ikawa, M. (2017). Human globozoospermia-related
855 gene spata16 is required for sperm formation revealed by CRISPR/Cas9-mediated mouse
856 models. *International Journal of Molecular Sciences*, *18*(10).
857 https://doi.org/10.3390/ijms18102208
858 Gamble, J., Chick, J., Seltzer, K., Graber, J. H., Gygi, S., Braun, R. E., & Snyder, E. M. (2020). An
859 expanded mouse testis transcriptome and mass spectrometry defines novel proteins.
860 *Reproduction, 159*(1), 15–26. https://doi.org/10.1530/REP-19-0092
861 Garrido-Martín, D., Borsari, B., Calvo, M., Reverter, F., & Guigó, R. (2021). Identification and analysis
862 of splicing quantitative trait loci across multiple tissues in the human genome. *Nature*
863 *Communications*, *12*(1). https://doi.org/10.1038/s41467-020-20578-2

Gebreyesus, G., Lund, M. S., Kupisiewicz, K., & Su, G. (2021). Genetic parameters of semen quality traits and genetic correlations with service sire nonreturn rate in Nordic Holstein bulls. *Journal of Dairy Science*, *104*(9), 10010–10019. https://doi.org/10.3168/jds.2021-20403

Giambartolomei, C., Vukcevic, D., Schadt, E. E., Franke, L., Hingorani, A. D., Wallace, C., & Plagnol, V. (2014). Bayesian Test for Colocalisation between Pairs of Genetic Association Studies Using Summary Statistics. *PLoS Genetics*, *10*(5). https://doi.org/10.1371/journal.pgen.1004383

GTEx Consortium. (2020). The GTEx Consortium atlas of genetic regulatory effects across human tissues. *Science*, *369*(6509), 1318–1330. www.gtexportal.org

Guo, J., Grow, E. J., Mlcochova, H., Maher, G. J., Lindskog, C., Nie, X., Guo, Y., Takei, Y., Yun, J., Cai, L., Kim, R., Carrell, D. T., Goriely, A., Hotaling, J. M., & Cairns, B. R. (2018). The adult human testis transcriptional cell atlas. *Cell Research, 28*(12), 1141–1157.

Guo, J., Nie, X., Giebler, M., Mlcochova, H., Wang, Y., Grow, E. J., Kim, R., Tharmalingam, M., Matilionyte, G., Lindskog, C., Carrell, D. T., Mitchell, R. T., Goriely, A., Hotaling, J. M., & Cairns, B. R. (2020). The Dynamic Transcriptional Cell Atlas of Testis Development during Human Puberty. *Cell Stem Cell*, *26*(2), 262-276.e4. https://doi.org/10.1016/j.stem.2019.12.005

Hiltpold, M., Kadri, N. K., Janett, F., Witschi, U., Schmitz-Hsu, F., & Pausch, H. (2021). Autosomal recessive loci contribute significantly to quantitative variation of male fertility in a dairy cattle population. *BMC Genomics*, *22*(1). https://doi.org/10.1186/s12864-021-07523-3

Hiltpold, M., Niu, G., Kadri, N. K., Crysnanto, D., Fang, Z. H., Spengeler, M., Schmitz-Hsu, F., Fuerst, C., Schwarzenbacher, H., Seefried, F. R., Seehusen, F., Witschi, U., Schnieke, A., Fries, R., Bollwein, H., Flisikowski, K., & Pausch, H. (2020). Activation of cryptic splicing in bovine WDR19 is associated with reduced semen quality and male fertility. *PLoS Genetics*, *16*(5). https://doi.org/10.1371/journal.pgen.1008804

Kaessmann, H. (2010). Origins, evolution, and phenotypic impact of new genes. In *Genome Research* (Vol. 20, Issue 10, pp. 1313–1326). https://doi.org/10.1101/gr.101386.109

Lamas-Toranzo, I., Hamze, J. G., Bianchi, E., Fernández-Fuertes, B., Pérez-Cerezales, S., Laguna-Barraza, R., Fernández-González, R., Lonergan, P., Gutiérrez-Adán, A., Wright, G. J., Jiménez-Movilla, M., & Bermejo-álvarez, P. (2020). TMEM95 is a sperm membrane protein essential for mammalian fertilization. *ELife*, *9*, 1–18. https://doi.org/10.7554/eLife.53913

Leonard, A. S., Crysnanto, D., Mapel, X. M., Bhati, M., & Pausch, H. (2023). Graph construction method impacts variation representation and analyses in a bovine super-pangenome. *Genome Biology*, *24*(1), 124. https://doi.org/10.1186/s13059-023-02969-y

896 Leonard, A. S., Mapel, X. M., & Pausch, H. (2023). Pangenome genotyped structural variation
897 improves molecular phenotype mapping in cattle. *BioRxiv*.
898 https://doi.org/10.1101/2023.06.21.545879
899 Li, H. (2013). *Aligning sequence reads, clone sequences and assembly contigs with BWA-MEM*.
900 http://arxiv.org/abs/1303.3997
901 Li, Y. I., Knowles, D. A., Humphrey, J., Barbeira, A. N., Dickinson, S. P., Im, H. K., & Pritchard, J. K.
902 (2018). Annotation-free quantification of RNA splicing using LeafCutter. *Nature Genetics*, *50*(1),
903 151–158. https://doi.org/10.1038/s41588-017-0004-9
904 Li, Y. I., Van De Geijn, B., Raj, A., Knowles, D. A., Petti, A. A., Golan, D., Gilad, Y., & Pritchard, J. K.
905 (2016). RNA splicing is a primary link between genetic variation and disease. *Science*,
906 *352*(6285), 600–604. https://www.science.org
907 Liao, Y., Smyth, G. K., & Shi, W. (2014). FeatureCounts: An efficient general purpose program for
908 assigning sequence reads to genomic features. *Bioinformatics*, *30*(7), 923–930.
909 https://doi.org/10.1093/bioinformatics/btt656
910 Liu, S., Gao, Y., Canela-Xandri, O., Wang, S., Yu, Y., Cai, W., Li, B., Xiang, R., Chamberlain, A. J., Pairo-
911 Castineira, E., D'Mellow, K., Rawlik, K., Xia, C., Yao, Y., Navarro, P., Rocha, D., Li, X., Yan, Z., Li,
912 C., … Fang, L. (2022). A multi-tissue atlas of regulatory variants in cattle. *Nature Genetics*, *54*(9),
913 1438–1447. https://doi.org/10.1038/s41588-022-01153-5
914 Liu, S., Ma, X., Wang, Z., Lin, F., Li, M., Li, Y., Yang, L., Rushdi, H. E., Riaz, H., Gao, T., Yang, L., Fu, T., &
915 Deng, T. (2023). MAEL gene contributes to bovine testicular development through the m5C-
916 mediated splicing. *IScience*, *26*(2). https://doi.org/10.1016/j.isci.2023.105941
917 Love, M. I., Huber, W., & Anders, S. (2014). Moderated estimation of fold change and dispersion for
918 RNA-seq data with DESeq2. *Genome Biology*, *15*(12). https://doi.org/10.1186/s13059-014-
919 0550-8
920 McLaren, W., Gil, L., Hunt, S. E., Riat, H. S., Ritchie, G. R. S., Thormann, A., Flicek, P., & Cunningham,
921 F. (2016). The Ensembl Variant Effect Predictor. *Genome Biology*, *17*(1).
922 https://doi.org/10.1186/s13059-016-0974-4
923 Mohammadi, P., Castel, S. E., Brown, A. A., & Lappalainen, T. (2017). Quantifying the regulatory
924 effect size of cis-acting genetic variation using allelic fold change. *Genome Research*, *27*(11),
925 1872–1884. https://doi.org/10.1101/gr.216747.116
926 Murat, F., Mbengue, N., Winge, S. B., Trefzer, T., Leushkin, E., Sepp, M., Cardoso-Moreira, M.,
927 Schmidt, J., Schneider, C., Mößinger, K., Brüning, T., Lamanna, F., Belles, M. R., Conrad, C.,
928 Kondova, I., Bontrop, R., Behr, R., Khaitovich, P., Pääbo, S., … Kaessmann, H. (2023). The

molecular evolution of spermatogenesis across mammals. *Nature*, *613*(7943), 308–316. https://doi.org/10.1038/s41586-022-05547-7

Nagai, R., Kinukawa, M., Watanabe, T., Ogino, A., Kurogi, K., Adachi, K., Satoh, M., & Uemoto, Y. (2022). Genome-wide detection of non-additive quantitative trait loci for semen production traits in beef and dairy bulls. *Animal*, *16*(3). https://doi.org/10.1016/j.animal.2022.100472

Oura, S., Koyano, T., Kodera, C., Yuki Horisawa-Takada, Matsuyama, M., Ishiguro, K. I., & Ikawa, M. (2021). KCTD19 and its associated protein ZFP541 are independently essential for meiosis in male mice. *PLoS Genetics*, *17*(5 May). https://doi.org/10.1371/journal.pgen.1009412

Pausch, H., Kölle, S., Wurmser, C., Schwarzenbacher, H., Emmerling, R., Jansen, S., Trottmann, M., Fuerst, C., Götz, K. U., & Fries, R. (2014). A Nonsense Mutation in TMEM95 Encoding a Nondescript Transmembrane Protein Causes Idiopathic Male Subfertility in Cattle. *PLoS Genetics*, *10*(1). https://doi.org/10.1371/journal.pgen.1004044

Pausch H, Mapel XM. Review: Genetic mutations affecting bull fertility. *Animal*, in press

Pirinen, M., Lappalainen, T., Zaitlen, N. A., Dermitzakis, E. T., Donnelly, P., McCarthy, M. I., & Rivas, M. A. (2015). Assessing allele-specific expression across multiple tissues from RNA-seq read data. *Bioinformatics*, *31*(15), 2497–2504. https://doi.org/10.1093/bioinformatics/btv074

Pockrandt, C., Alzamel, M., Iliopoulos, C. S., & Reinert, K. (2020). GenMap: Ultra-fast computation of genome mappability. *Bioinformatics, 36*(12), 3687–3692. https://doi.org/10.1093/bioinformatics/btaa222

Poplin, R., Chang, P. C., Alexander, D., Schwartz, S., Colthurst, T., Ku, A., Newburger, D., Dijamco, J., Nguyen, N., Afshar, P. T., Gross, S. S., Dorfman, L., McLean, C. Y., & Depristo, M. A. (2018). A universal snp and small-indel variant caller using deep neural networks. *Nature Biotechnology*, *36*(10), 983. https://doi.org/10.1038/nbt.4235

Ramsköld, D., Wang, E. T., Burge, C. B., & Sandberg, R. (2009). An abundance of ubiquitously expressed genes revealed by tissue transcriptome sequence data. *PLoS Computational Biology*, *5*(12). https://doi.org/10.1371/journal.pcbi.1000598

Rezende, F. M., Dietsch, G. O., & Peñagaricano, F. (2018). Genetic dissection of bull fertility in US Jersey dairy cattle. *Animal Genetics*, *49*(5), 393–402. https://doi.org/10.1111/age.12710

Robertson, M. J., Kent, K., Tharp, N., Nozawa, K., Dean, L., Mathew, M., Grimm, S. L., Yu, Z., Légaré, C., Fujihara, Y., Ikawa, M., Sullivan, R., Coarfa, C., Matzuk, M. M., & Garcia, T. X. (2020). Large-scale discovery of male reproductive tract-specific genes through analysis of RNA-seq datasets. *BMC Biology, 18*(1). https://doi.org/10.1186/s12915-020-00826-z

Rosen, B. D., Bickhart, D. M., Schnabel, R. D., Koren, S., Elsik, C. G., Tseng, E., Rowan, T. N., Low, W. Y., Zimin, A., Couldrey, C., Hall, R., Li, W., Rhie, A., Ghurye, J., McKay, S. D., Thibaud-Nissen, F.,

Hoffman, J., Murdoch, B. M., Snelling, W. M., … Medrano, J. F. (2020). De novo assembly of the cattle reference genome with single-molecule sequencing. *GigaScience*, *9*(3). https://doi.org/10.1093/gigascience/giaa021

Saha, A. & Battle, A. (2019) False positives in trans-eQTL and co-expression analyses arising from RNA-sequencing alignment errors [version 2; peer review: 3 approved]. *F1000Research*, 7:1860 https://doi.org/10.12688/f1000research.17145.2

Smit, AFA., Hubley, R. & Green, P. *RepeatMasker Open-4.0*. 2013-2015. http://www.repeatmasker.org

Soumillon, M., Necsulea, A., Weier, M., Brawand, D., Zhang, X., Gu, H., Barthès, P., Kokkinaki, M., Nef, S., Gnirke, A., Dym, M., deMassy, B., Mikkelsen, T. S., & Kaessmann, H. (2013). Cellular Source and Mechanisms of High Transcriptome Complexity in the Mammalian Testis. *Cell Reports*, *3*(6), 2179–2190. https://doi.org/10.1016/j.celrep.2013.05.031

Stegle, O., Parts, L., Piipari, M., Winn, J., & Durbin, R. (2012). Using probabilistic estimation of expression residuals (PEER) to obtain increased power and interpretability of gene expression analyses. *Nature Protocols*, *7*(3), 500–507. https://doi.org/10.1038/nprot.2011.457

Tang, S., Lu, Y., Skinner, W. M., Sanyal, M., Lishko, P. V, Ikawa, M., & Kim, P. S. (2022). Human sperm TMEM95 binds eggs and facilitates membrane fusion. *Biophysics and computational biology open access*. https://doi.org/10.1073/pnas

Tarasov, A., Vilella, A. J., Cuppen, E., Nijman, I. J., & Prins, P. (2015). Sambamba: fast processing of NGS alignment formats. *Bioinformatics*, *31*(12), 2032–2034. https://doi.org/10.5281/zenodo.13200

The FarmGTEx-PigGTEx Consortium, Teng, J., Gao, Y., Yin, H., Bai, Z., Liu, S., Zeng, H., Bai, L., Cai, Z., Zhao, B., Xu, Z., Lin, Q., Pan, Z., Yang, W., Yu, X., Hou, Y., Keel, B. N., Rohrer, G. A., Lindholm-Perry, A. K., … Fang, L. (2022). A compendium of genetic regulatory effects across pig tissues. *BioRxiv*. https://doi.org/10.1101/2022.11.11.516073

Thibier, M., & Wagner, H.-G. (2002). World statistics for artificial insemination in cattle. In Livestock Production Science (Vol. 74). www.elsevier.com/locate/livprodsci

Tüttelmann, F., Ruckert, C., & Röpke, A. (2018). Spermatogenesestörungen: Perspektiven für erweiterte genetische Diagnostik nach 20 Jahren unveränderter Routine. Medizinische Genetik, 30(1), 12–20. https://doi.org/10.1007/s11825-018-0181-7

Urbut, S. M., Wang, G., Carbonetto, P., & Stephens, M. (2019). Flexible statistical methods for estimating and testing effects in genomic studies with multiple conditions. *Nature Genetics*, *51*(1), 187–195. https://doi.org/10.1038/s41588-018-0268-8

Van De Geijn, B., Mcvicker, G., Gilad, Y., & Pritchard, J. K. (2015). WASP: Allele-specific software for robust molecular quantitative trait locus discovery. In *Nature Methods* (Vol. 12, Issue 11, pp. 1061–1063). Nature Publishing Group. https://doi.org/10.1038/nmeth.3582

Wainberg, M., Sinnott-Armstrong, N., Mancuso, N., Barbeira, A. N., Knowles, D. A., Golan, D., Ermel, R., Ruusalepp, A., Quertermous, T., Hao, K., Björkegren, J. L. M., Im, H. K., Pasaniuc, B., Rivas, M. A., & Kundaje, A. (2019). Opportunities and challenges for transcriptome-wide association studies. *Nature Genetics*, *51*(4), 592–599. https://doi.org/10.1038/s41588-019-0385-z

Walker, R. L., Ramaswami, G., Hartl, C., Mancuso, N., Gandal, M. J., de la Torre-Ubieta, L., Pasaniuc, B., Stein, J. L., & Geschwind, D. H. (2019). Genetic Control of Expression and Splicing in Developing Human Brain Informs Disease Mechanisms. *Cell*, *179*(3), 750-771.e22. https://doi.org/10.1016/j.cell.2019.09.021

Wang, S., Qiao, H., Wang, P., Wang, Y., & Qin, D. (2021). ZDHHC19 is dispensable for spermatogenesis, but is essential for sperm functions in mice. *International Journal of Molecular Sciences*, *22*(16). https://doi.org/10.3390/ijms22168894

Wang, W., Su, L., Meng, L., He, J., Tan, C., Yi, D., Cheng, D., Zhang, H., Lu, G., Du, J., Lin, G., Zhang, Q., Tu, C., & Tan, Y.-Q. (2023). Biallelic variants in KCTD19 associated with male factor infertility and oligoasthenoteratozoospermia. *Human Reproduction*. https://doi.org/10.1093/humrep/dead095

Wu, Y., Broadaway, K. A., Raulerson, C. K., Scott, L. J., Pan, C., Ko, A., He, A., Tilford, C., Fuchsberger, C., Locke, A. E., Stringham, H. M., Jackson, A. U., Narisu, N., Kuusisto, J., Pajukanta, P., Collins, F. S., Boehnke, M., Laakso, M., Lusis, A. J., … Mohlke, K. L. (2019). Colocalization of GWAS and eQTL signals at loci with multiple signals identifies additional candidate genes for body fat distribution. *Human Molecular Genetics*, *28*(24), 4161–4172. https://doi.org/10.1093/hmg/ddz263

Xavier, M. J., Salas-Huetos, A., Oud, M. S., Aston, K. I., & Veltman, J. A. (2021). Disease gene discovery in male infertility: past, present and future. In Human Genetics (Vol. 140, Issue 1, pp. 7–19). Springer Science and Business Media Deutschland GmbH. https://doi.org/10.1007/s00439-020-02202-x

Xiang, R., Fang, L., Liu, S., Macleod, I. M., Liu, Z., Breen, E. J., Gao, Y., Liu, G. E., Tenesa, A., Consortium, C., Mason, B. A., Chamberlain, A. J., Wray, N. R., & Goddard, M. E. (2022). Gene expression and RNA splicing explain large proportions of the heritability for complex traits in cattle. *BioRxiv*. https://doi.org/10.1101/2022.05.30.494093

Yamaguchi, K., Ishigaki, K., Suzuki, A., Tsuchida, Y., Tsuchiya, H., Sumitomo, S., Nagafuchi, Y., Miya, F., Tsunoda, T., Shoda, H., Fujio, K., Yamamoto, K., & Kochi, Y. (2022). Splicing QTL analysis

1030 focusing on coding sequences reveals mechanisms for disease susceptibility loci. *Nature*
1031 *Communications*, *13*(1). https://doi.org/10.1038/s41467-022-32358-1
1032 Yang, J., Lee, S. H., Goddard, M. E., & Visscher, P. M. (2011). GCTA: A tool for genome-wide complex
1033 trait analysis. *American Journal of Human Genetics*, *88*(1), 76–82.
1034 https://doi.org/10.1016/j.ajhg.2010.11.011
1035 Yun, T., Li, H., Chang, P. C., Lin, M. F., Carroll, A., & McLean, C. Y. (2020). Accurate, scalable cohort
1036 variant calls using DeepVariant and GLnexus. *Bioinformatics*, *36*(24), 5582–5589.
1037 https://doi.org/10.1093/bioinformatics/btaa1081
1038 Zhang, Y., Liu, Z., Yun, X., Batu, B., Yang, Z., Zhang, X., Zhang, W., & Liu, T. (2023). Transcriptome
1039 Profiling of Developing Testes and First Wave of Spermatogenesis in the Rat. *Genes, 14*(1).
1040 https://doi.org/10.3390/genes14010229
1041